



Multiple intensifications inside the auroral bulge and their association with plasma sheet activities

A. Keiling,¹ V. Angelopoulos,¹ D. Larson,¹ J. McFadden,¹ C. Carlson,¹ M. Fillingim,¹ G. Parks,¹ S. Frey,¹ K.-H. Glassmeier,² H. U. Auster,² W. Magnes,³ W. Liu,⁴ and X. Li⁴

Received 9 May 2008; revised 15 October 2008; accepted 29 October 2008; published 31 December 2008.

[1] In this coordinated ground and space study, we report multiprobe measurements from Time History of Events and Macroscale Interactions during Substorms (THEMIS), LANL-97A, Polar, and ground observatories for a substorm that occurred on 23 March 2007. The THEMIS fleet and LANL-97A were located in the premidnight, near-Earth plasma sheet in the radial range from 6.6 to 13 R_E , placing the spacecraft into different plasma environments which were subject to different activities. Simultaneous global Polar Ultraviolet Imager images of the aurora revealed a fine structure in the auroral bulge in the form of several time-delayed regions of brightening. We demonstrate a correspondence between this fine structure and the spatially separated plasma sheet activities (substorm injections with energies >100 keV) by showing that both executed periodic (100–150 s) one-to-one correlated modulations. Additionally, the different auroral brightening regions were modulated approximately out of phase to one another, as were the separated plasma sheet activities. The periodic plasma sheet and optical modulations were also one-to-one correlated with large-amplitude ($\delta H \sim 150$ nT) ground Pi2 pulsations. In contrast to the most energetic ions (>100 keV), the lower-energetic plasma sheet ions executed separate oscillations during the development of the substorm, including the preintensification phase, and showed the following properties. (1) The oscillation periods were different at different spacecraft locations and had a tendency to increase during the evolution of the substorm. During the preintensification phase, multiple (possibly harmonic) spectral components existed. (2) The oscillations were coupled to westward moving perturbations of an energized plasma boundary. The boundary perturbations were likely conjugate to azimuthally spaced auroral forms (“beads”) observed by Polar-UVI during the preintensification phase and could play a role in the onset of the substorm intensification. (3) The oscillations of the lower-energetic ions were also one-to-one correlated with smaller-amplitude ground Pi2 pulsations (<15 nT). In conclusion, the combination of these observations allowed us to construct a 3-D picture of low-frequency, near-Earth plasma sheet phenomena associated with a substorm and their connection to aurora and the ground. It appeared that not only one substorm current wedge, but additional current structures existed which started at different times, pulsated out of phase, and mapped from different active regions into the ionosphere. The active space regions appeared to be coupled and transferring energy from one region to the other while pulsating. We propose that the wave-like structures in the plasma sheet, observed before and during the substorm/intensification phase, and their demonstrated properties support a wave phenomenon (such as a ballooning-type mode) for the onset and development of the substorm/intensification, rather than directly driven periodic bursty bulk flow activations.

Citation: Keiling, A., et al. (2008), Multiple intensifications inside the auroral bulge and their association with plasma sheet activities, *J. Geophys. Res.*, 113, A12216, doi:10.1029/2008JA013383.

¹Space Sciences Laboratory, University of California, Berkeley, California, USA.

²Technische Universität Braunschweig, Braunschweig, Germany.

³Space Research Institute, Austrian Academy of Science, Graz, Austria.

⁴Laboratory for Atmospheric and Space Physics, University of Colorado, Boulder, Colorado, USA.

1. Introduction

[2] The occurrence of low-frequency, magnetohydrodynamic (MHD) waves near the inner edge of the plasma sheet, in association with substorms, is well known [e.g., Roux *et al.*, 1991; Cheng, 1991; Bauer *et al.*, 1995b; Holter *et al.*, 1995; Erickson *et al.*, 2000]. In addition, it is

recognized that small-scale, kinetic effects are crucial in understanding substorm onset [e.g., *Lui et al.*, 1999]. Some evidence suggests that substorm onset is a wave phenomenon associated with a kinetic/MHD instability, leading to the disruption of the cross-tail current and dipolarization (see review by *Lui* [1996]). Auroral breakup is the ionospheric manifestation of this process. The simplest auroral onset begins at one localized region in the ionosphere and then rapidly expands in longitude and latitude. The initial auroral expansion can be followed by additional auroral intensifications, quickly leading to a large area covered by aurora. The evolution of this auroral spreading can best be observed from global auroral images and has been documented in many studies. However, the exact relationship between the waves in space, a possible kinetic/MHD instability, and their manifestations in ground/ionospheric signatures has not been conclusively established.

1.1. Near-Earth Wave Phenomena

[3] Several features of wave activity associated with substorm onset in the near-Earth plasma sheet, mainly observed from single spacecraft measurements, have been identified. In the late 1980s, it was recognized that substorm onsets are associated with large-amplitude magnetic field fluctuations in the near-Earth plasma sheet [e.g., *Takahashi et al.*, 1987]. *Lui et al.* [1992] interpreted these fluctuations as temporal structures associated with substorm onset, as opposed to the erratic crossing of a spatial structure (e.g., X line). The magnetic fluctuations encompass low- to high-frequency components [e.g., *Lui and Najmi*, 1997]. High-frequency components are thought to be associated with the mechanism disrupting the current sheet, while low-frequency components are possibly associated with a MHD instability [e.g., *Miura et al.*, 1989; *Roux et al.*, 1991; *Cheng*, 1991; *Ohtani and Tamao*, 1993; *Bhattacharjee et al.*, 1998; *Cheng and Lui*, 1998] or driven by bursty bulk flows (BBFs) coming from the magnetotail [e.g., *Angelopoulos et al.*, 1994].

[4] Different interpretations for the nature of the waves in the near-Earth plasma sheet have been given. For example, *Bauer et al.* [1995a] identified plasma sheet oscillations with 1–2 min periods near the neutral sheet during the expansion phase of substorms. This type of wave was reported to be maintained in the vicinity of the neutral sheet, and did not occur in the growth or recovery phases of substorms. The fluctuation amplitude was comparable to the background magnetic field and the compressional component dominated. Additionally, proton and electron pressure fluctuations were in anti-phase with the magnetic field oscillations, which led the authors to interpret them as the motion of the inhomogeneous plasma sheet passing the spacecraft, and as a transient response of the plasma sheet to the formation of the substorm current wedge. It was further suggested, not experimentally confirmed, that the fluctuations are related to ground Pi2 pulsations. The authors also pointed out the simultaneous occurrence of high-speed plasma flows.

[5] In a case study, *Roux et al.* [1991] interpreted magnetic field oscillations at geosynchronous distance as a westward propagating wave resulting from an Alfvén-ballooning instability, and suggested that this instability is the cause of and coupled to the westward traveling surge. In

this scenario, the azimuthal and northward expansions of the aurora were said to be due to the expansion of this instability in the plasma sheet. However, since only single spacecraft measurements were available, this scenario could not be confirmed. *Holter et al.* [1995] reanalyzed the same substorm-associated oscillations/waves, first reported by *Roux et al.* [1991], and found oscillations with different periods. During early breakup, field oscillations had periods of 45 s and 65 s followed by oscillations with a period of ~300 s. It was suggested that the long-period wave occurred on entire field lines, while the short-period waves were trapped in a current layer which developed prior to the substorm breakup. Additionally, there was some evidence that the long-period wave was a second harmonic mode. Both studies reported an out-of-phase relationship between particles and the compressional component of the waves. *Holter et al.* [1995] interpreted this relationship as the signature for coupled shear Alfvén-slow mode waves, a fundamentally different interpretation from the one given by *Bauer et al.* [1995a]. The diamagnetic relationship in the boundary motion case [*Bauer et al.*, 1995a] is simply due to the convection of the inhomogeneous plasma, whereas for the slow mode it is due to compression and rarefaction of the plasma.

[6] *Lui and Najmi* [1997] noted the broad range of frequencies at substorm breakup, in a case study as well, and that some higher-frequency components shifted in frequency continuously to lower frequencies, an observation also reported by *Holter et al.* [1995]. Several studies have reported waves before substorm onset and suggested a possible role of these waves in initiating substorms. *Ohtani et al.* [1992] reported the explosive growth of a magnetic field perturbation before onset, believed to be due to a sudden increase of the cross-tail current. *Cheng and Lui* [1998] argued that an oscillation already starts one to two wave periods earlier and is associated with a kinetic ballooning instability. *Erickson et al.* [2000] distinguished between oscillations, called trigger waves by the authors, of the electric (60–90 s) and magnetic field (30 s) before explosive growth, and suggested that they play a role in initiating the explosive growth phase.

1.2. Manifestation on the Ground and in the Ionosphere

[7] The connection between near-Earth phenomena and their manifestations in ground/ionospheric signatures has been intensely studied but with limited results. Some ground magnetic field oscillations are believed to be caused by plasma sheet oscillations/waves in the near-Earth plasma sheet [e.g., *Bauer et al.*, 1995a]. Substorm-associated high-latitude ground oscillations have been associated with the onset of the substorm current wedge (SCW) which launches Alfvén waves toward the ionosphere [e.g., *Maynard et al.*, 1996; *Erickson et al.*, 2000]. It has been argued that some wave energy reflects back to the plasma sheet, causing a “ringing” of the flux tubes due to the mismatch between the conductance of the flux tube and the reflecting boundary, a scenario known as the transient response model [e.g., *Baumjohann and Glassmeier*, 1984]. Most of the evidence for this scenario comes from ground observations; in particular, one-to-one correlations of in situ SCW-associated Alfvén waves and ground oscillations have not been

reported. A different scenario relates the fluctuations of a growing and oscillating instability in the near-Earth plasma sheet to ground oscillations [e.g., Cheng, 2004]. For this scenario, the frequency is not due to the bounce time of Alfvén waves but is controlled by the instability.

[8] Regarding the auroral signature, Roux *et al.* [1991] argued that the site of the ballooning instability in the near-Earth plasma sheet is the cause of and conjugate to the westward traveling surge in the ionosphere. To date, there have been no additional observations confirming this connection. Thirty years ago, it was noted that the westward traveling surge is not always a continuous progression but occurs in discrete steps [Sergeev and Yahnin, 1979]. Also suggested was that individual auroral intensifications could be connected to different regions in space [e.g., Sergeev, 1974], a suggestion that has never been confirmed through observations. Another manifestation of plasma sheet oscillations/waves is thought to be in the form of azimuthally spaced auroral forms just before onset. For 26 out of 37 substorms, Elphinstone *et al.* [1995] reported the existence of these structures before the explosive poleward motion, with azimuthal mode numbers, m , ranging between 30 and 135 (i.e., the number of wavelengths that would fit into 2π rad). Shear flows and wave instabilities in the near-Earth plasma sheet have been invoked as possible causes for these auroral forms [Elphinstone *et al.*, 1995; Murphree and Johnson, 1996; Friedrich *et al.*, 2001] (see section 7 for additional information on the ballooning mode).

[9] Field line resonance (FLR) has been shown to cause magnetic field pulsations on the ground. There is ample ground-based evidence of nightside FLR activity in the 1–4 mHz band on field lines that map from the CPS [e.g., Samson *et al.*, 1991; Ruohoniemi *et al.*, 1991; Ziesolleck and McDiarmid, 1994]. In particular, FLR activity has been recorded near the inner edge of the CPS [e.g., Hughes and Grard, 1984; Keiling *et al.*, 2001; Samson *et al.*, 2003] some of which was substorm-related. One class of auroral arcs has been shown to be luminously modulated by FLR. Most studies have utilized ground-based optical and magnetic field measurements to establish this relationship [e.g., Rankin *et al.*, 1999; Wanliss and Rankin, 2002]. Lessard *et al.* [1999] reported space observations of an FLR that modulated conjugate aurora. In this study, the authors concluded that substorm onset, which occurred before the FLR observation, was not the cause of the FLR, and that a solar wind source was more probable. In general, the role of FLR in the substorm process has not been established, although it has been suggested that they may trigger an instability that leads to substorm onset [e.g., Samson *et al.*, 1992].

[10] An improved understanding of the substorm trigger mechanism and the spreading of substorm-associated phenomena in space requires simultaneous observations at multiple points in space. Where and how onset occurs and evolves is the primary objective of the five-spacecraft Time History of Events and Macroscale Interactions during Substorms (THEMIS) mission [Angelopoulos, 2008; Sibeck and Angelopoulos, 2008]. In this study, we utilized in situ measurements from THEMIS and LANL-97A to analyze wave phenomena of low-frequency (<0.03 Hz) magnetic field and particle oscillations in the near-Earth plasma sheet during the 23 March 2007 substorm, and their manifestation

on the ground/ionosphere in the form of magnetic pulsations and optical signatures. Our study complements other studies [Angelopoulos *et al.*, 2008; Raeder *et al.*, 2008; Keiling *et al.*, 2008; Liu *et al.*, 2008] which analyzed related phenomena associated with the same substorm. The results reported here demonstrate the variability of field and particle oscillations due to both temporal and spatial effects during this substorm, and provide observational evidence that different active regions of space were connected with different brightening regions inside the auroral bulge, as depicted in Figure 1. Correlations with magnetometer data are also established.

2. Instrumentation

[11] The observations presented here are from the five THEMIS satellites [Angelopoulos, 2008; Sibeck and Angelopoulos, 2008; Bester *et al.*, 2008], the THEMIS magnetometer ground stations [Russell *et al.*, 2008], the 210 MM magnetometer network [Yumoto and the 210° MM Magnetic Observation Group, 1996], the geosynchronous LANL-97A satellite, and the Polar satellite. Each THEMIS spacecraft consists of an identical set of instruments. For this study, we incorporated data from the solid state telescope (D. Larson *et al.*, Solid state telescope for THEMIS, submitted to *Space Science Reviews*, 2008), the electrostatic analyzer [McFadden *et al.*, 2008], and the fluxgate magnetometer [Auster *et al.*, 2008]. Data from the electric field instrument (J. W. Bonnell *et al.*, The electric field instrument (EFI) for THEMIS, submitted to *Space Science Reviews*, 2008) were not available. Data from the LANL-97A spacecraft included the energetic particles flux from the SOPA (Synchronous Orbit Particle Analyzer) instrument. The magnetic field vector was sampled at 1/3 Hz (spin resolution) and 4 Hz. Together, both particle detectors (ESA and SST) provide an energy range from a few eV to ~500 keV for ions at a time resolution of 3 s. The time resolution of ground magnetometer data was 2 Hz (for THEMIS) and 1 Hz (for 210 MM). In addition, we used the Ultraviolet Imager (UVI) on Polar [Torr *et al.*, 1995] with a cadence of 37 s, which provided the global morphology of the aurora.

3. Overview

[12] On 23 March 2007 a substorm occurred while the THEMIS fleet was located in the premidnight plasma sheet at 8 to 13 R_E (geocentric distance). The five spacecraft were in a string-of-pearls configuration (following each other on similar equatorial orbits with an apogee of 15.4 R_E) in the following order: TH-C, D, B, A, and E (Figure 2). As seen in Figure 2, probes TH-A, B, and D were the closest together (~1000 km); and the leading TH-C and trailing TH-E were approximately 2–3 R_E away from other spacecraft in the fleet. At the time of the substorm, the UVI on board Polar monitored the global development of the aurora (Figure 3). In this section we briefly point out the main features, and provide more detail later, together with in situ observations for each data set. As identified by Angelopoulos *et al.* [2008], three auroral activations can be identified for the 23 March 2007 event. The first activation occurred at ~1054 UT (2100–2300 MLT) and showed a faint, elongated structure (image 1), which could possibly be classified as a pseudo-

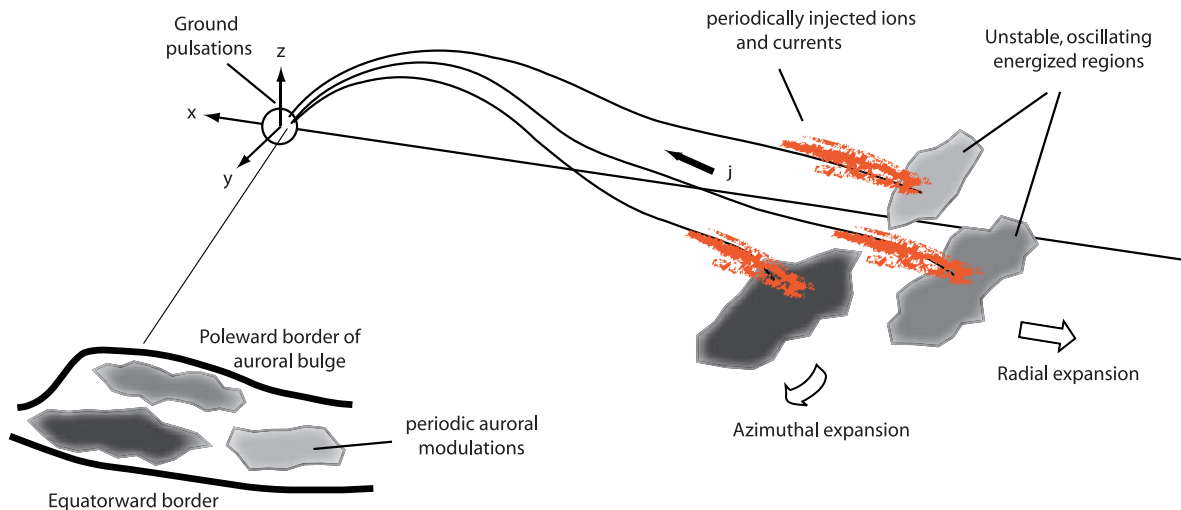


Figure 1. Scenario showing the magnetic connections between largely separated regions (ionosphere and the near-Earth plasma sheet). The bottom part shows a schematic of the auroral bulge, as observed on 23 March 2007, during its expansion. Three separate structures can be identified (the design of the inset was adapted from *Kenell [1995]* and applied to the 23 March 2007 substorm). Each auroral structure is conjugate to a different region in space that drives low-altitude signatures, such as auroral modulations and ground magnetic field pulsations.

breakup that subsequently faded. At ~ 1109 UT farther to the east at ~ 0100 MLT (image 3), the first onset brightening (breakup) occurred (second activation), followed by a modest expansion poleward and westward (image 4, etc.). At the 1109 UT onset, the first activation site at 2100–2200 MLT simultaneously intensified (images 4 and 5). During the expansion of the brightening region, azimuthally spaced auroral structures (image 4) formed west of the expanding auroral bulge which turned into a faint, elongated auroral structure (image 6). The faint structure abruptly and greatly intensified (third activation) at ~ 1119 UT (2300 MLT; image 8) with even more luminosity than during the first breakup, marking the beginning of the first intensification phase. Important to note is the fact that the substorm intensification was not a continuous expansion of the smaller substorm onset farther east, but an activation at a new location. After the first intensification, the auroral bulge showed additional time-delayed auroral intensifications at new locations inside the bulge (images 9 and 10).

[13] During this substorm, the foot points of the THEMIS spacecraft were located inside the ellipse (Figure 3, image 2) which coincides with the location of the auroral intensifications. Mapping was partially based on the MHD simulation by *Raeder et al. [2008]* using the Open Geospace General Circulation Model (OpenGGCM), and on a comparison of corresponding in situ and ground signatures (as discussed subsequently). Therefore, THEMIS was suitably located to monitor the conditions inside the near-Earth plasma sheet during both the preintensification and the intensification phase. As shown below, THEMIS was not directly in the current disruption region but slightly below it and only periodically entered the active plasma region.

[14] In addition to the global auroral signatures, the various activations also manifested themselves in the ground magnetic field data (Figure 4). The first two panels show, as a reference, the global auroral development of the substorm in the form of keograms from Polar UVI. A subset

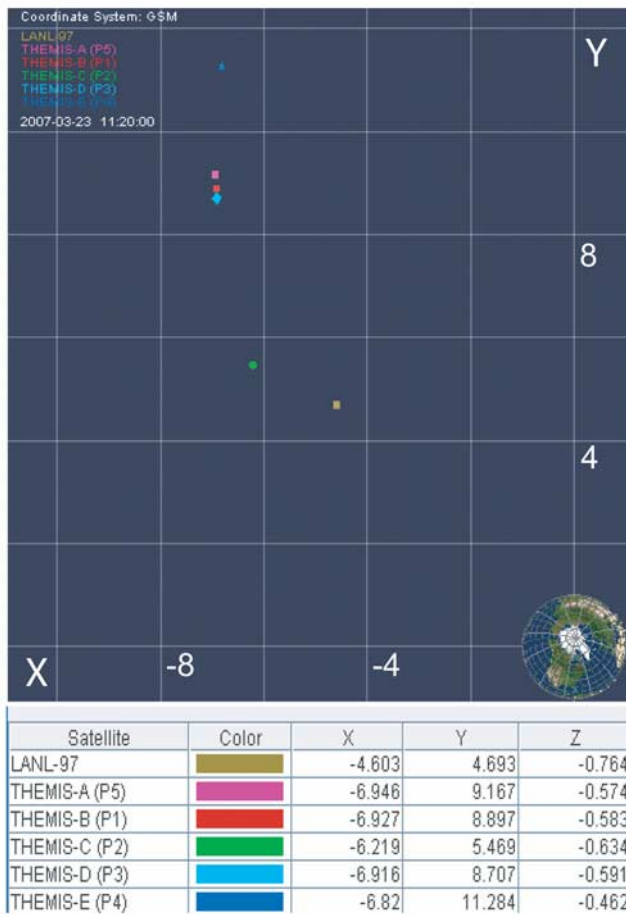


Figure 2. Positions (in R_E) of the THEMIS and LANL-97A spacecraft in the X-Y (GSM) plane on 23 March 2007 at 1120 UT. Software is provided by <http://sscweb.gsfc.nasa.gov/tipsod>.

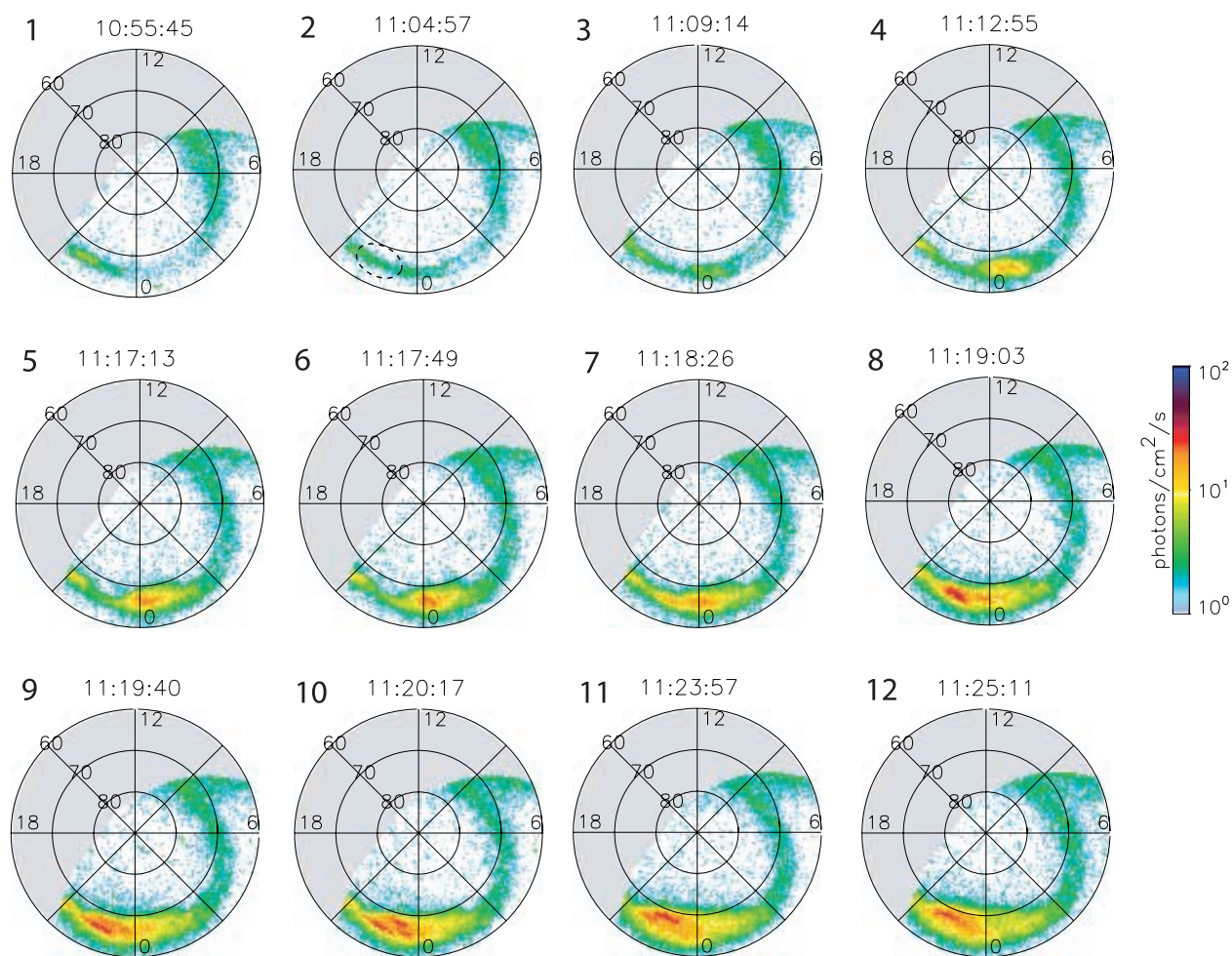


Figure 3. Several UVI images from the Polar spacecraft showing parts of the substorm development on 23 March 2007. The second image shows the proximate vicinity (ellipse) of the spacecraft footprints for all THEMIS and LANL-97A spacecraft at ~ 1120 UT.

of magnetograms (FSIM, FSMI, and KIAN; spanning ~ 3 h in local time) shows at least three activations (see vertical lines in Figures 4c–4e) which likely correspond to the auroral activations described in the previous paragraphs. The substorm onset, as seen in the H component of ground magnetometer, occurred near FSIM (ground station in western Canada) and expanded westward. The auroral intensification can also be seen in the sharp drop in H at KIAN, which was located west of FSIM and FSMI (compare to Figure 4b showing the abrupt auroral intensification approximately between 22 and 23 MLT). KIAN also recorded Pi2 pulsations before and after the intensification onset (Figure 4e).

[15] Similar to ground observations, three activation onsets could be identified in space in the form of magnetic field fluctuations/oscillations and particle flux modulations recorded by THEMIS, which was in the plasma sheet throughout the 23 March 2007 substorm. Each spacecraft, however, recorded different onset times and different oscillation signatures (see dashed lines in Figures 4f–4j), except for TH-D, B, and A which recorded very similar signatures due to spatial closeness. The first sign of enhanced fluctua-

tions occurred at 1053 UT as recorded by TH-C, and at 1058 UT as recorded by the other spacecraft (first dashed line from left in each panel), approximately coinciding with an increase in the magnetic field intensity at TH-C, D, and B. Noted here is that B_y contributed most to the magnetic field intensity due to the orientation of \mathbf{B} . The second activation (second dashed line) was seen first at TH-D, B, and A, and later at TH-C (compare to Figure 7). Finally, the third activation (third dashed line) was recorded as a weak dipolarization at TH-D, B, A, and possibly as a time-delayed observation (spike in B_z) by TH-E. Although TH-C recorded clear signatures of enhanced fluctuations, no dipolarization was recorded.

[16] The different onsets in magnetic field activity also found their counterparts in the particle signatures. Figure 5 shows differential ion flux (>28 keV) from all five THEMIS spacecraft, plus LANL-97A, ordered by magnetic local time (top, farthest east; bottom, farthest west; compare to Figure 2). The time interval encompasses the onset and the multiple intensifications, leaving out the pseudobreakup (first activation) which was only recorded for lower-energy particles. TH-D, B, and A again recorded very similar

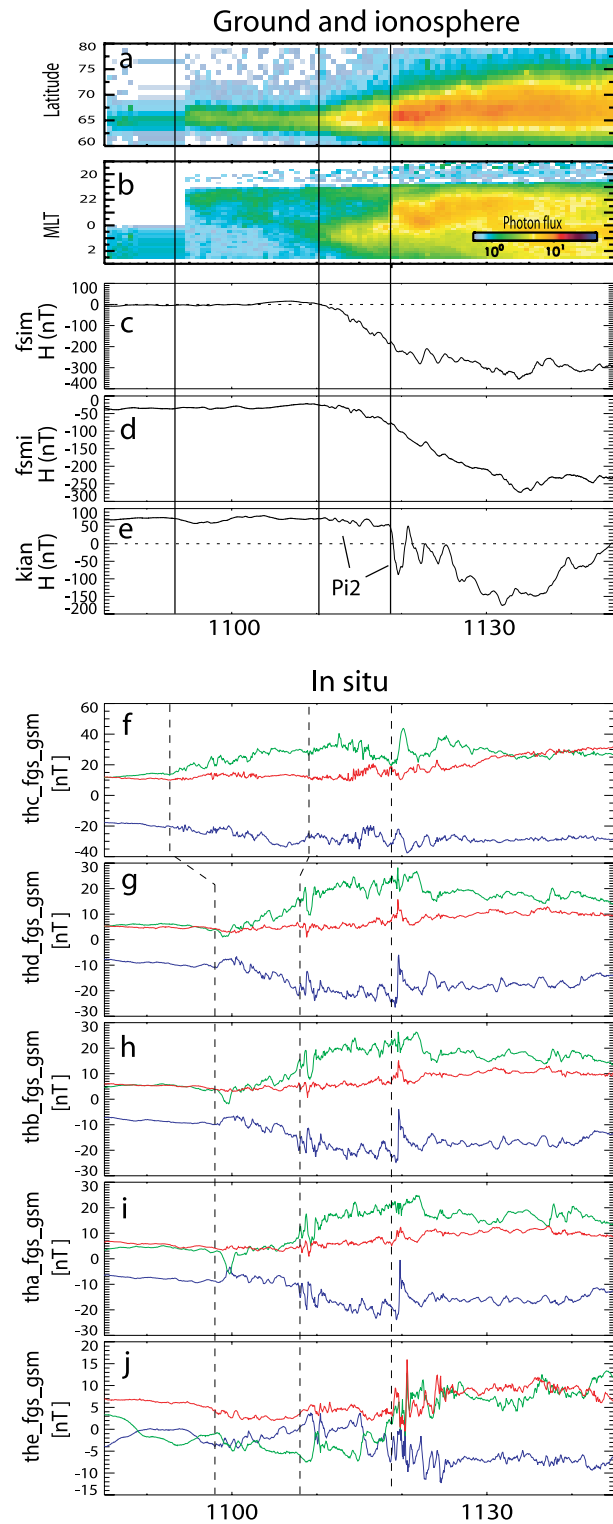


Figure 4. Selected in situ, ground magnetometer, and optical data from the 23 March 2007 substorm. (a and b) Keograms from Polar-UVI; (c–e) magnetometer data from Fort Simpson (61.8° latitude, 238.8° longitude geographic), Fort Smith, and Kiana (66.97° latitude, 199.56° longitude geographic); and (f–j) unfiltered magnetic field data from five THEMIS spacecraft (in GSM coordinates), where vertical dashed lines indicate the onset times of space activations. Spacecraft are ordered by east-west locations: top, farthest east; bottom, farthest west.

signatures owing to their close positions, while TH-C, E, and LANL-97A recorded significant differences. Owing to the similarities among some spacecraft, we grouped the spacecraft into two groups (Group 1, Group 2), as indicated in Figure 5. In Group 1, both spacecraft recorded intense ion injections starting at ~1120 UT. While ion injections at TH-C were dispersionless, those at LANL-97A showed a clear dispersion in different energy channels (see dashed lines). On the other hand, LANL-97A did not record the preintensification oscillations (between 1110 and 1120 UT) which were very pronounced at TH-C. The signatures in Group 2 are significantly different from those of Group 1. Within Group 2 there are smaller differences as well; in particular, TH-E shows the least similarity. Around 1120 UT it appears that the first ion injection was recorded by TH-E as a dispersed signature. TH-D, B, and A, on the other hand, recorded almost dispersionless injections. However, at a later time (e.g., last dashed line), there appeared to be no dispersion among all spacecraft of Group 2. Additionally, TH-E did not record the preintensification oscillations which were clearly visible at TH-D, B, and A. Some additional similarities were found, mostly at higher-energy

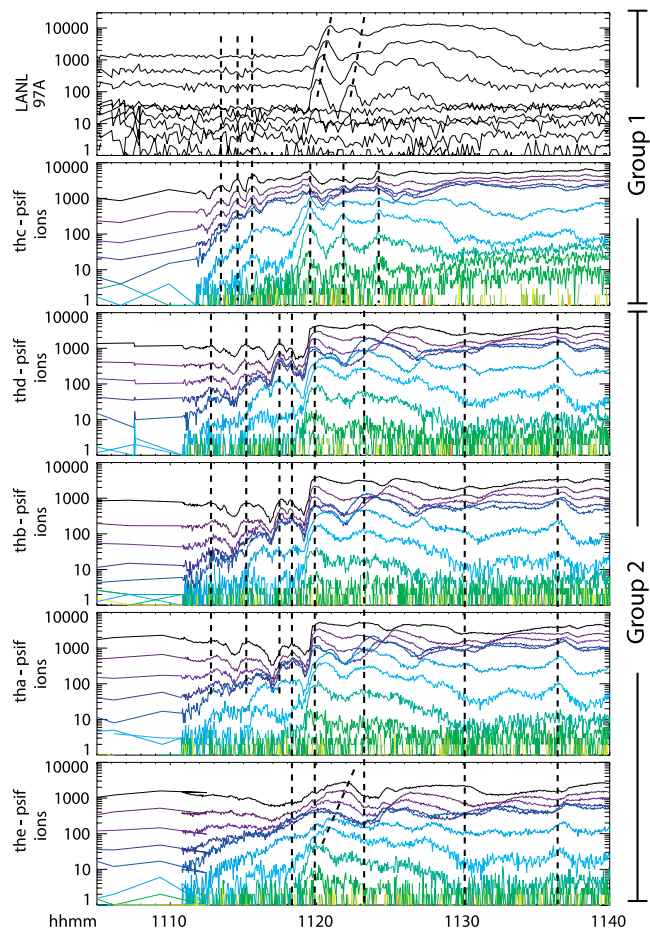


Figure 5. Ion energy flux from LANL-97A and all THEMIS spacecraft. The energy ranges are 75–400 keV and 28–395 keV for LANL-97A and THEMIS, respectively. Vertical lines emphasize similarities between individual structures, as further explained in the text.

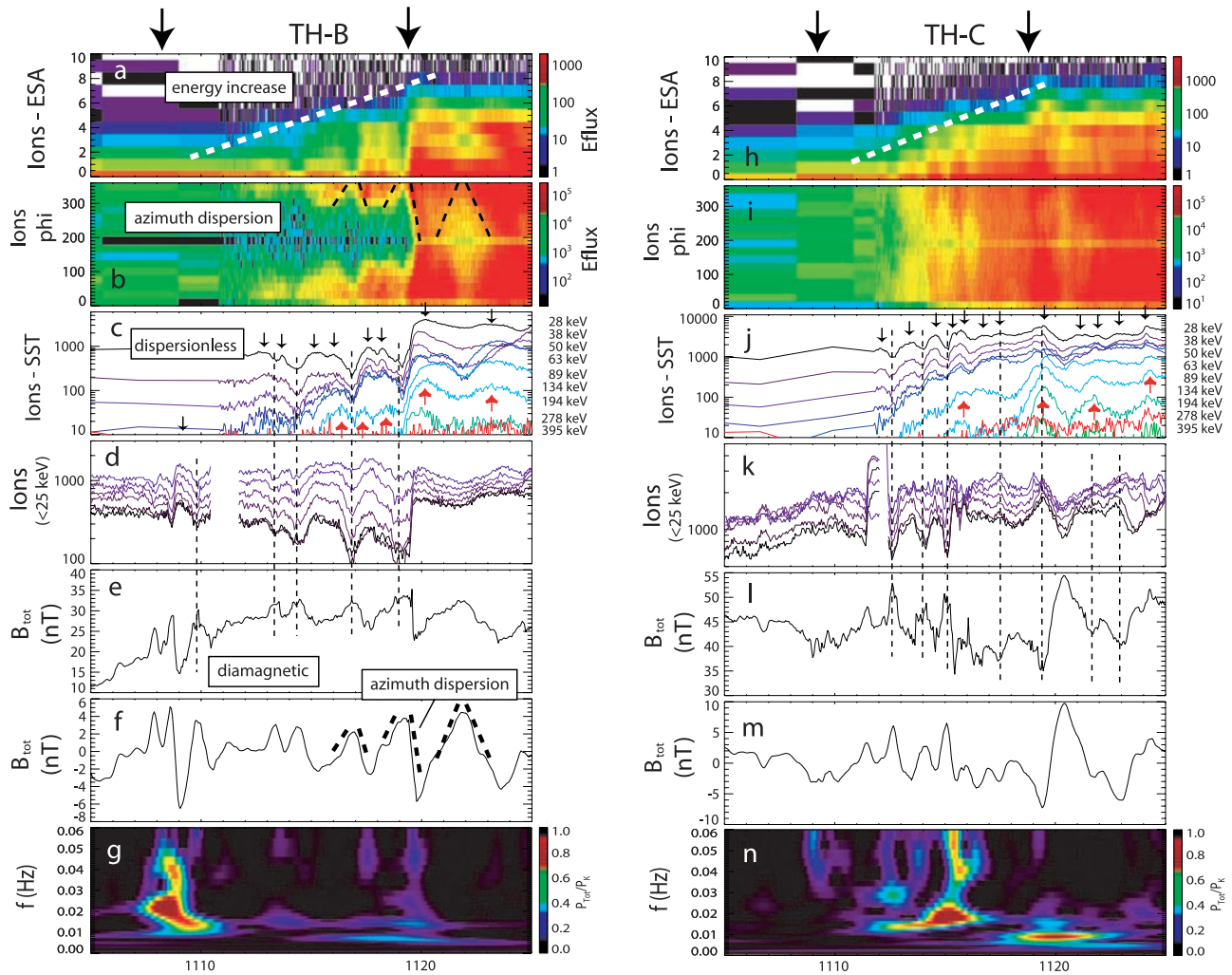


Figure 6. Particle and magnetic field data during the 23 March 2007 substorm from TH-B and TH-C. (a) Ion energy-time spectrogram; (b) ion azimuth spectrogram as a proxy for pitch angle spectrogram; (c and d) ion differential flux covering the energy range from a few eV to ~ 395 keV; (e) unfiltered; (f) filtered magnetic field strength; (g) the wavelet power spectrum of total B. (h – n) Same as Figures 6a–6g but for TH-C.

channels (bottom lines, light green and light blue), among all Group 2 spacecraft. Additional time delay effects exist at TH-D, B, and A, and will be discussed in more detail in the following sections.

[17] The inter-spacecraft and ground-spacecraft comparisons described in this section indicate that the spacecraft not only recorded temporal variations due to the substorm development, but also spatial variations due to their physical separation. We divided the six spacecraft into two groups, which were located in two distinct plasma environments. In the following sections, we show more detailed comparisons of spacecraft data (section 4), optical data (section 5), and ground magnetometer data (section 6).

4. Spacecraft Observations

[18] In section 3 we indicated that TH-D, B, and A (Group 2) recorded very similar signatures that were different from those recorded by TH-C and LANL-97A (Group 1). Figure 6 shows expanded views of magnetic field and particle

data from TH-B and TH-C (each a representative of their respective group). The arrows above the first panel of each spacecraft approximately indicate the onset times of enhanced preintensification ion flux oscillations and of very energetic (>100 keV) ion injections. The oscillations during the preintensification phase showed periods of ~ 3 min and 1–2 min for TH-B and C, respectively. In addition, the oscillations were superposed by shorter-period oscillations, seen clearly for TH-B (see small black arrows in the third panel) and seen vaguely for TH-C (see arrows at ~ 1116 UT). Also apparent from Figure 6 is that the energies of oscillating ions increase up to the intensification onset (white dashed line in the first panel for each probe). Ions with energies less than 100 keV experienced different modulations than those with energies greater than 100 keV (see downward and upward pointing arrows in the third panel for each spacecraft), which suggests that the acceleration mechanism was energy dependent. No time delay between different energy channels (vertical dashed lines) is visible. The dispersionless signature can be explained with the periodic entering and

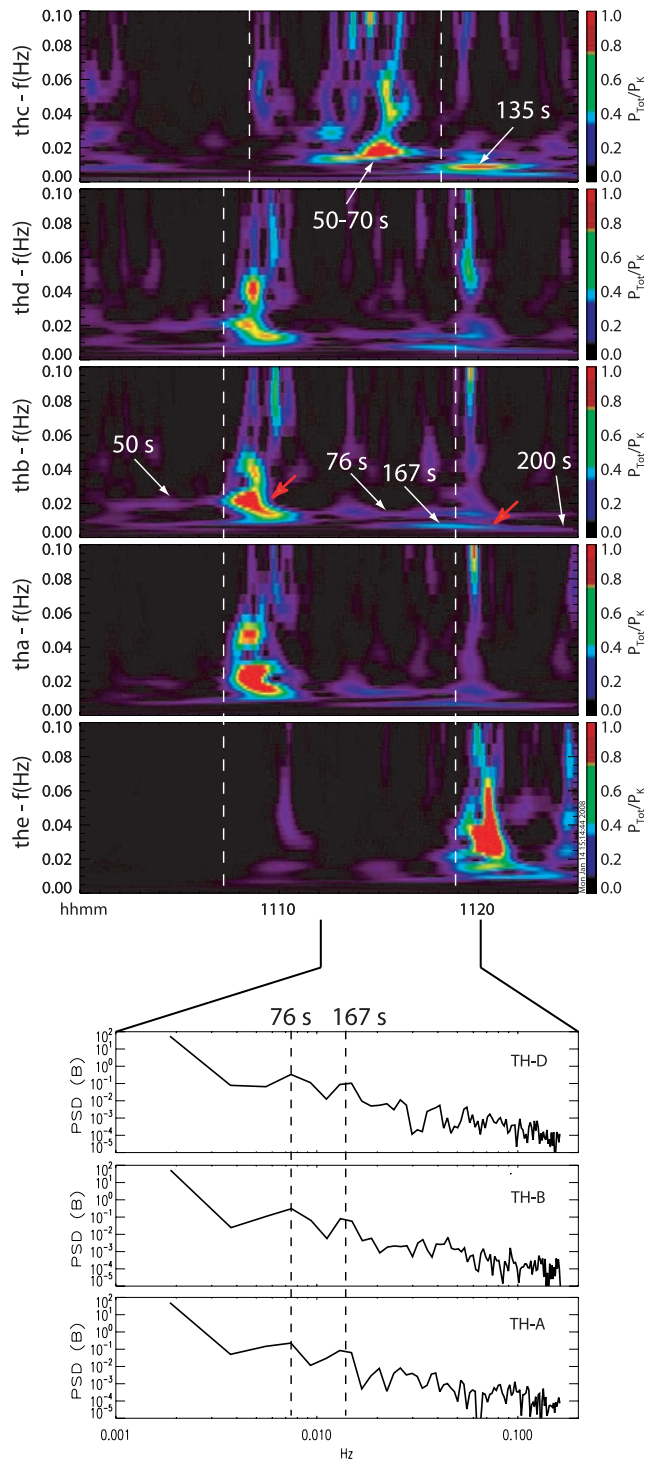


Figure 7. (top) Wavelets power spectra of the total magnetic field for all THEMIS spacecraft. Vertical dashed lines indicate the times of two activation signatures in space (compare to Figure 4). (bottom) Fourier transform of the total magnetic field for TH-D, B, and A during the time interval 1112–1120 UT.

leaving of a region of energized plasma. This periodic motion can be inferred, among other signatures (see below), from the azimuth spectrogram (second panel for each spacecraft) which shows that each flux enhancement is associated with

a dispersion in the azimuth (outlined by dashed lines). Owing to the magnetic field and particle sensor orientation, the azimuth is nearly equivalent to the pitch angle during this particular time interval. The azimuth angles 130° and 310° approximately correspond to the field-aligned and anti-field-aligned direction. Using remote sensing, *Angelopoulos et al.* [2008] showed that the azimuth dispersion, for the intensification at 1119 UT on TH-B (second arrow above first panel), corresponded to the crossing of a boundary, which was horizontally layered and moved at a speed of about 70 km/s southward (i.e., lobeward). A similar argument could be applied to the modulations before the intensification, noting that for this case the spacecraft appear only partially

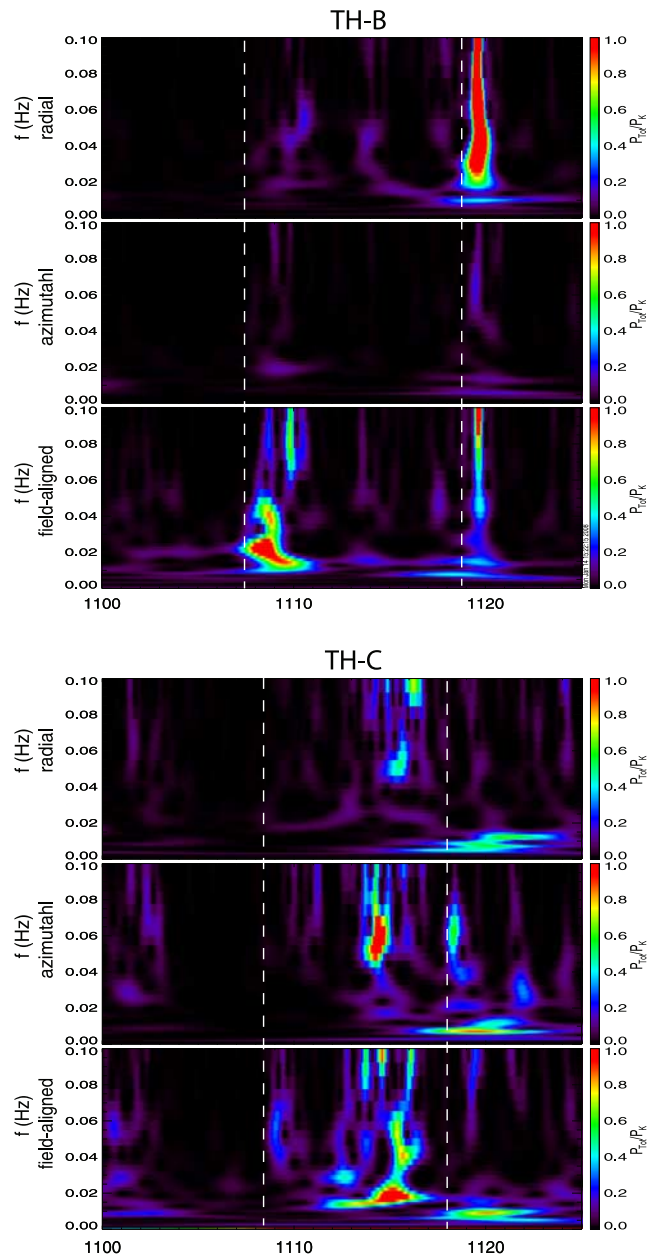


Figure 8. Wavelets power spectra of the three magnetic field components, in field-aligned coordinates, for TH-B and TH-C. The vertical dashed lines indicate the times of two activations in space (compare to Figure 6).

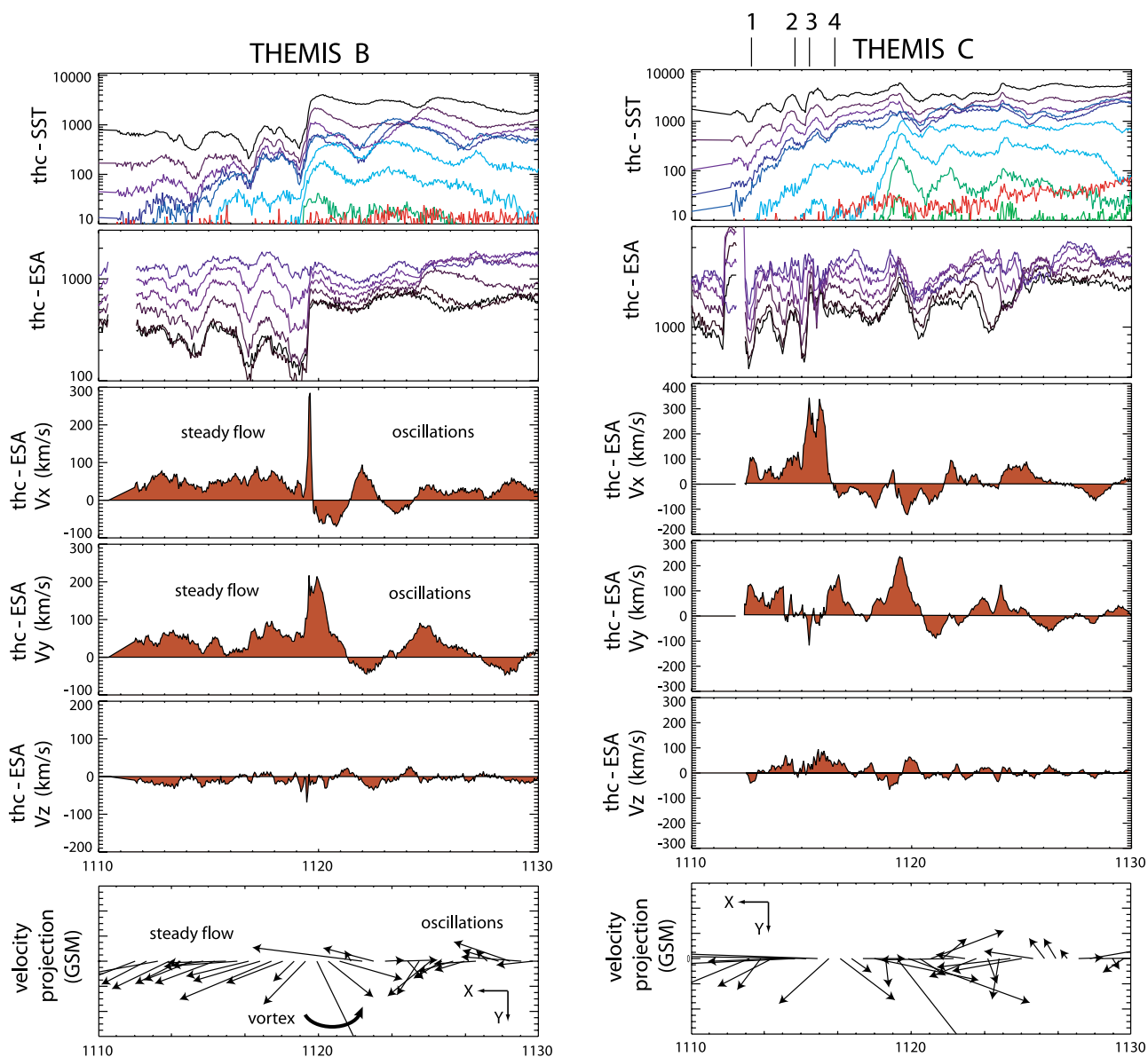


Figure 9. Ion energy flux (compare to Figure 6) and ion velocity from TH-B and TH-C. The last panel for each spacecraft shows the projection of the bulk velocity vector onto the X-Y (GSM) plane. Numbered lines above the first panel of TH-C indicate the times for UVI images shown in Figure 13.

immersed in the energized boundary layer, since the particles' azimuth had not yet isotropized. Also noted is the fact that an opposite azimuth dispersion indicates a boundary motion in the opposite direction.

[19] The fifth and sixth panels show the unfiltered and filtered total magnetic field, showing oscillations with dB/B of $\sim 35\%$ and $\sim 15\%$ for TH-B and TH-C, respectively. The magnetic oscillations are out of phase by 180° with the oscillations of the particle flux. As pointed out by Keiling *et al.* [2008] for TH-C, the magnetic perturbations for the 23 March 2007 event were largely controlled by the boundary motion of the lower-energetic plasma (<100 keV) but not the energetic (>100 keV) ion injections. The diamagnetic relationship is due to the spacecraft entering and exiting the region of energized plasma, as was inferred in the previous paragraph. To emphasize this interpretation, we have overlaid the magnetic field with the dashed lines from Figure 6b

(azimuth dispersion) in Figure 6f (TH-B). With changing azimuth, the spacecraft probes ions with different pitch angle, and, therefore, penetrates more or less deeply into the boundary layer; as a result, the total magnetic field gets weaker or stronger in diamagnetic fashion. A similar boundary motion interpretation can be given for the recorded particle and field data of TH-C.

[20] Although the boundary motion recorded by TH-B and TH-C was qualitatively similar, the periods of oscillations and onset times differed quantitatively. To further investigate these differences, wavelet power spectra of the total magnetic field strength of all THEMIS spacecraft were employed (Figure 7). It is noted that the total magnetic field is, at the same time, a representation of the particle flux modulations due to the diamagnetic relationship, as described above. As expected, TH-D, B, and A (which were closest to each other) recorded very similar signatures. The

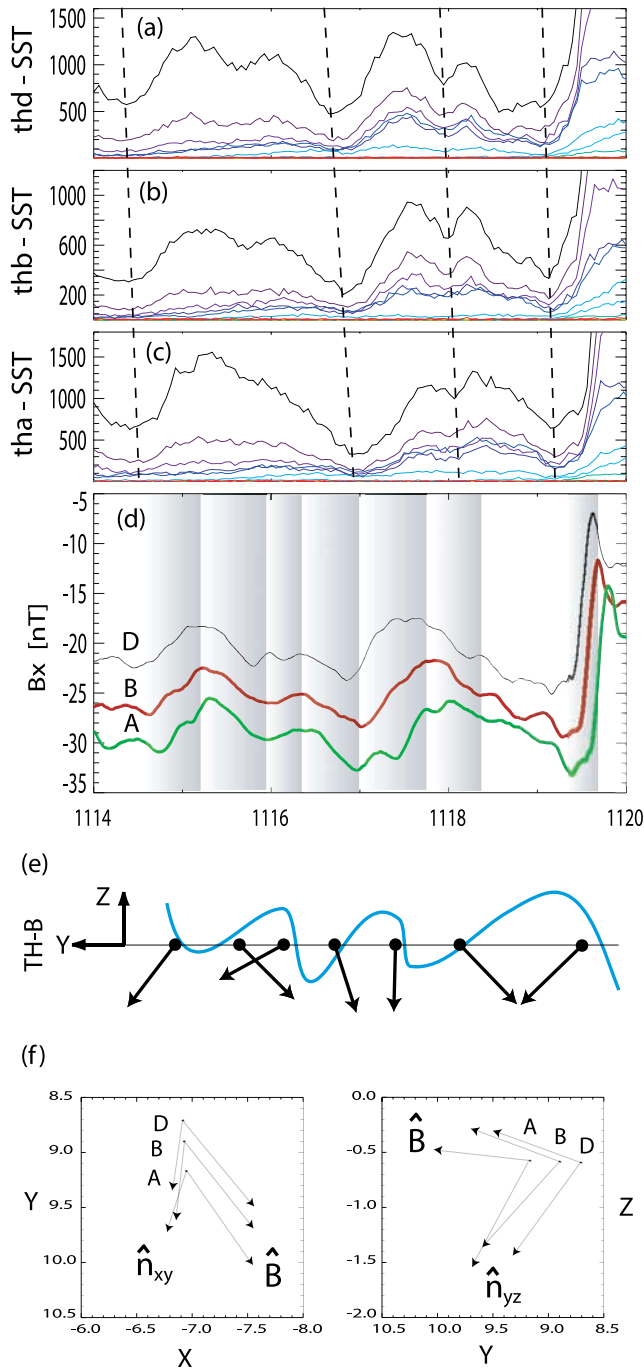


Figure 10. Boundary analysis for the three closely spaced THEMIS spacecraft. (a–c) Ion energy flux for individual energy channels. (d) B_x component of the magnetic field for TH-D (black), TH-B (red), and TH-A (green). (e) Projections of the MVA directions onto the Y-Z (GSM) plane for TH-B. Each vector is centered on a shaded region in Figure 10d, which was used for the MVA analysis. The blue wavy line illustrates the perturbations on the boundary. (f) Projections of the boundary normal and background magnetic field direction onto two planes for the time interval corresponding to the shaded region on the far right in Figure 10d.

first and second vertical dashed lines mark the onset of activations and correspond to the times indicated by arrows in Figure 6. Here, our discussion again focuses on TH-C and TH-B (representatives of the two groups defined in section 3), which recorded distinctly different signatures. Immediately before the first activation (first dashed line from the left), TH-B recorded oscillations in the Pi2 range, ~ 50 s, which then intensified at first activation, followed by an increase in period to approximately 76 s. The oscillation continued until, and beyond, the second activation (second dashed line). In addition, a second lower-frequency oscillation was observed with a period of 167 s before the intensification. The Fourier transform (shown at the bottom of Figure 7) for the time interval 1112–1120 UT confirmed that two prominent spectral peaks at 76 s and 167 s were present at TH-B, D, and A. The ratio of both periods suggests that they are harmonically related. After the intensification, the previous oscillations continued for TH-B. While the 76-s oscillation remained unchanged, the 167-s oscillation shifted to a lower period of 200 s. A similar frequency shift was noted above for the first activation (at the first dashed line). Both shifts are marked by red arrows and can be seen enlarged in Figure 6g, which shows the same quantity expanded. As already indicated above in the description of Figure 6, the transition from preintensification to intensification (~ 1120 UT) did not disrupt the low-frequency waves, in spite of the sharp broadband pulse caused by the dipolarization at the spacecraft's locations. The oscillations recorded by TH-C also changed during the course of the substorm but were distinctly different from those recorded by TH-B. Before the first activation (first dashed line) there were no Pi2-like oscillations. Shortly after the first activation, TH-C recorded an oscillation with a period of 50–70 s, followed by a 135-s oscillation associated with the intensification (second dashed line). In order to determine the wave polarization, we calculated the wavelet power spectra of the three magnetic field components (in field-aligned coordinates) for TH-B and TH-C. As seen in Figure 8 for the low-frequency component (<0.03 Hz) considered here, the compressional component (B_z) dominated until the intensification (second dashed line). At the time of intensification, the radial (B_x) and toroidal (B_y) components (<0.03 Hz) contributed considerably, which we attribute to field-aligned currents initiated at intensification.

[21] Figure 9 shows velocity moments during the preintensification and intensification phase. For reference, we have repeated the ion energy fluxes which show oscillations that were associated with the north-south motion of an energized plasma. The velocity moments show the strongest flows in the X-Y (GSM) plane and relatively small flows in the Z (GSM) direction. Three different types of behaviors (steady flow, vortex, and sloshing), which were associated with different activation phases, can be identified for the X-Y flows. During the preintensification phase the flow was unidirectional and azimuthally westward with speeds of <150 km/s (combining V_x and V_y) for TH-B. The preintensification flow was suddenly interrupted at ~ 1119 UT by a large transient flow enhancement (~ 360 km/s) in the same direction as the steady flow. It was followed by a flow (<150 km/s), largely in the X-Y plane, that sloshed back and forth (~ 3 -min period) for several periods. The flow direction is also illustrated in the flow vector plot in the last

panel, first showing a fairly steady flow in one direction and then what appears to be a flow vortex (rotation of the flow vector) followed by an oscillating sloshing motion. The vortex coincided with the onset of the intensification (intense ion injections) at TH-B (see first and second panels). The rotational sense was clockwise (i.e., positive vortex). The plasma flows recorded by TH-C were similar to those of TH-B, except that at TH-C the fastest flow (~ 350 km/s) occurred several minutes before the main ion injections (onset of intensification) and at TH-B it occurred at the time of the ion injections. Before the intense flow, the flow velocity was on the order of ~ 150 km/s, as it was for TH-B, and showed variations possibly associated with a velocity shear layer. The sloshing motion started immediately after the intense flow. For comparison, the numbered lines above the first panel of TH-C indicate the times of UVI images (see section 5).

[22] So far, we have contrasted the differences among the two groups of spacecraft. The similarities among TH-D, B and A, on the other hand, allow us the determination of propagation speeds for disturbances. A close inspection of the preintensification oscillations and the first intensification in the expanded view (Figures 10a–10d) points to time delays between the three spacecraft for both magnetic field and particle data (e.g., see dashed lines), indicating that the disturbances propagated westward. TH-D recorded the disturbance first, followed by TH-B (5-s delay) and TH-A (11-s delay). All three spacecraft were approximately located along a line $\sim 0.6 R_E$ below the nominal neutral sheet (Figure 10f). Owing to this configuration, we were restricted to a determination of the propagation (phase) speed in this specific direction. The direction is at an approximate 45° angle to the background magnetic field, which predominantly lies in the X-Y (GSM) plane. Using the separations of the spacecraft and the corresponding time delays, we found propagation (phase) speeds of 237 km/s and 281 km/s. These speeds should be considered upper limits. For a comparison, using Figure 9, we inferred an azimuthal flow speed of <150 km during the preintensification phase. We also found that flux modulations were due to a periodic entering and existing of the spacecraft into an energized plasma. A comparison of particle data from three closely aligned spacecraft (Figures 10a–10c) shows that the energized plasma was entered and exited first by the same spacecraft rather than entered first and exited last by the same spacecraft. This pattern suggests that the particle and field perturbations correspond to bulges in the boundary of the energized plasma moving past the spacecraft. This scenario can be confirmed with a minimum variance analysis (MVA) [Sonnerup and Cahill, 1968] applied to separate time intervals that correspond to the entering (decreasing $|B_x|$) and existing (increasing $|B_x|$) into the energized plasma. (A similar analysis was applied to so-called current sheet flappings [e.g., Runov et al., 2003; Sergeev et al., 2003]). In Figure 10d, these time intervals are highlighted by shaded bars indicating the beginning and ending of the interval. Determined MVA directions, with intermediate to minimal eigenvalue ratios ranging between 2.5 and 30, correspond to the normal direction of the oscillating boundary and are shown in Figure 10e as projections into the Y-Z (GSM) plane. The alternating directions of the normal vector in the +Y and -Y direction are due to the passing

of several boundary perturbations (i.e., boundary waves) and are schematically illustrated by the wavy blue line in Figure 10e. It is noted, however, that the normal directions are not entirely in the Y-Z plane, and also vary in the X direction. Therefore, the wave-like perturbations or bulges result in a more complicated 3-D pattern than is illustrated in Figure 10e. Figure 10f shows an example of the normal vector (from MVA analysis) in two planes for all three spacecraft, associated with the boundary perturbations of the intensification (first shaded region from the right in Figure 10d), and the direction of the background magnetic field.

5. Conjugate Aurora

[23] During the substorm the UVI on board Polar monitored the development of the aurora. THEMIS foot points were west of the first onset region (Figure 11, image 1; also see Figure 3 for the foot point mapping). In section 3 we identified an intensification onset at approximately 1119 UT (Figure 11, images 3 and 4), which is also clearly visible in the photon flux from UVI-Polar (top of Figure 11, first panel, solid red line, bearing in mind the cadence of the imager). The photon flux was averaged over the local time sector 2100–0000 MLT at 65° latitude, covering the region of auroral intensification. In image 5, at 68° – 69° , a second large-scale auroral structure appeared which can be seen in the photon fluxes (top of Figure 11, second and third panels), averaged from 68° to 69° (2100–0000 MLT). When compared to the first auroral structure, the onset (green line) of the second auroral structure was delayed by one image. The photon flux intensities (first three panels) show modulations with a period of approximately 100–150 s (see dashed lines). Two additional features in the photon fluxes are worth noting: First, the two regions at 65° and 68° – 69° oscillated out of phase, and, second, while the lower brightening region at 65° decreased in intensity, the upper brightening region at 68° – 69° increased in intensity. These intensity variations can also be seen (although not as easily) in individual UVI images (not shown) that follow image 6 in Figure 11. The reader should be aware that the longitudinal extent of the elongated auroral structures associated with each intensification (Figure 11, images 4, 5, and 6) is not reliable owing to the wobble of the Polar spacecraft, which artificially stretches structures in the direction of the wobble. Nevertheless, the separation between individual structures is clearly visible and is not an artifact.

[24] Figure 12 shows a comparison of ion energy fluxes recorded by TH-C, TH-B, and TH-D; and the averaged photon fluxes from global UVI images. The photon flux plots are identical to those shown in Figure 11. In the second, sixth, and seventh panels, single energy channels are shown to facilitate the comparison with the averaged photon fluxes. The modulations of the averaged photon flux after the intensification onset line up with those of the ion energy fluxes (dashed lines). Furthermore, the onsets of both auroral intensification and ion injections coincided, allowing for the time resolution of the UVI. The reader should also note that it is the higher-energetic particles (>100 keV) that correlated with the auroral modulations. These correlations suggest that the spacecraft were conjugate to individual structures inside the auroral bulge. In Figure 11 (image 6), one can identify a separate third

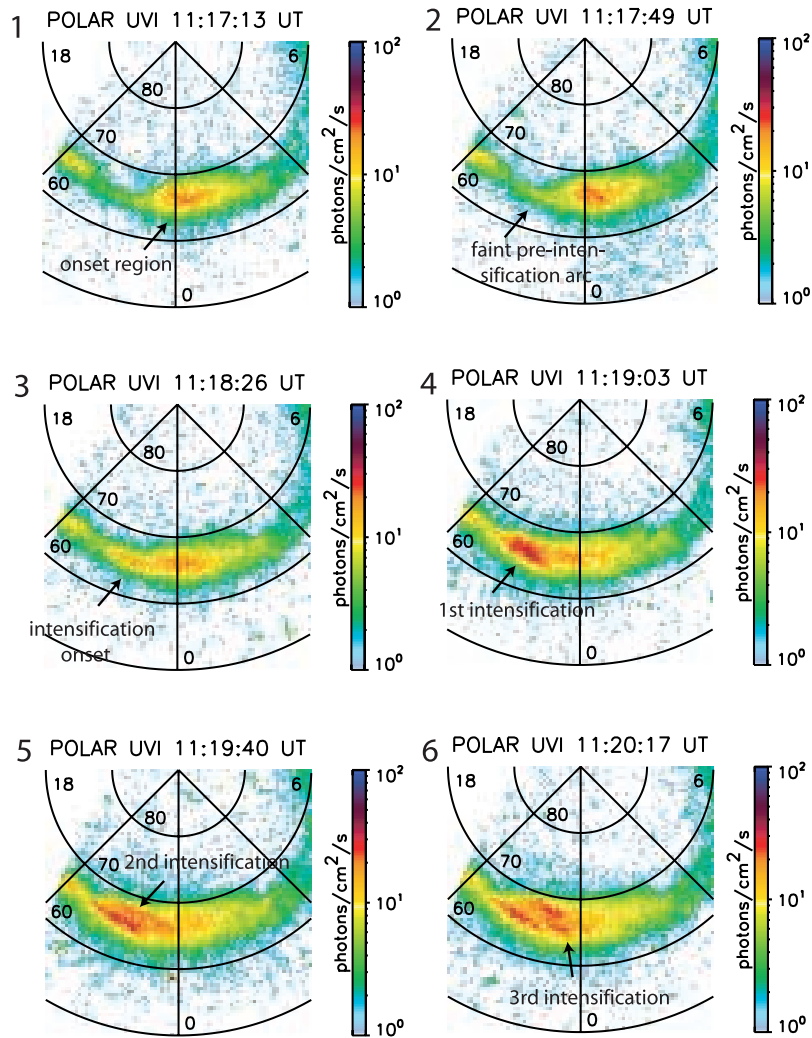
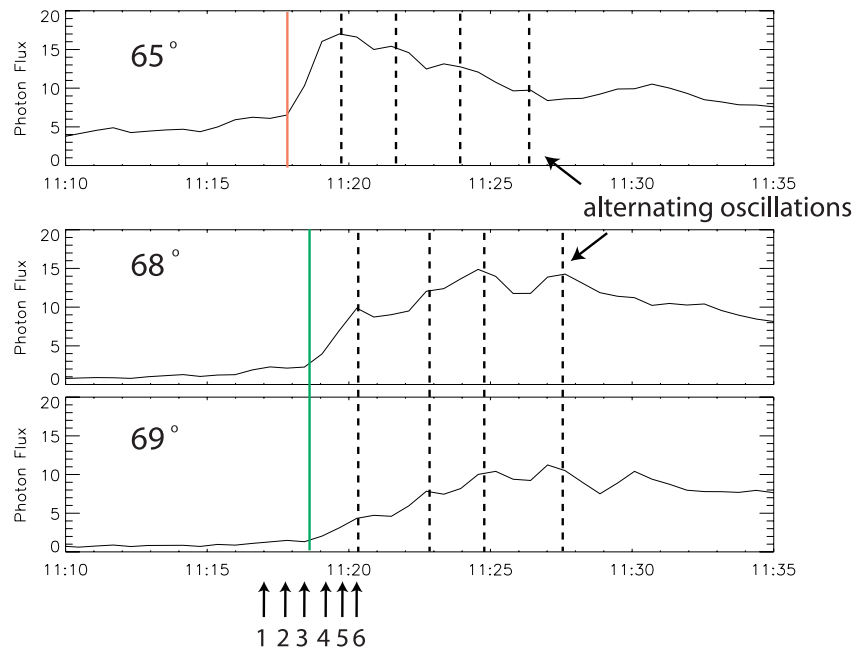
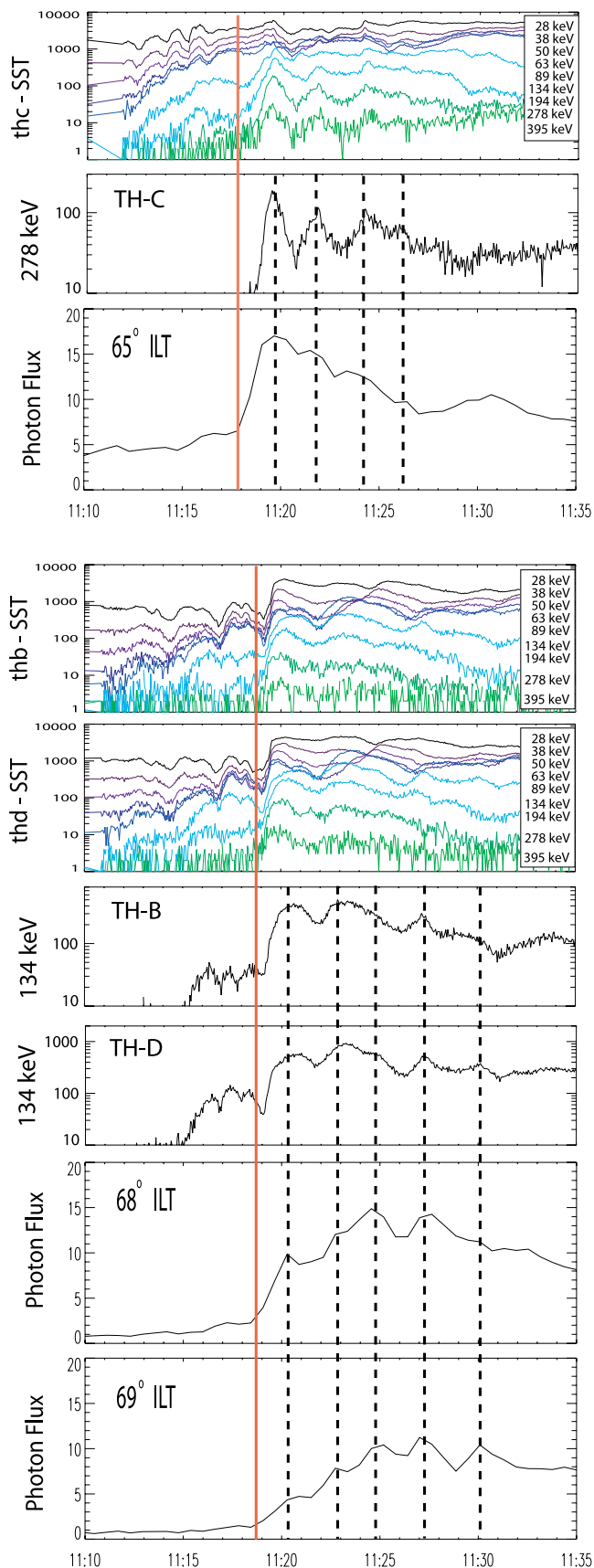


Figure 11. (top) Averaged photon fluxes spanning the local sector 2100–0000 MLT for three different latitudes. (bottom) Sequence of UVI images. The time of each image is indicated by arrows beneath the third panel at the top.



structure inside the auroral bulge. However, no spacecraft appeared to be conjugate; therefore, no comparison with in situ measurements could be done.

[25] Before onset of the first intensification, a faint auroral structure, possibly one or several arcs, existed at the same location ($\sim 65^\circ$ latitude) where the intensification occurred (Figure 11, image 2). A closer look (Figure 13) revealed that this structure initially showed additional fine structure in the azimuthal direction. Such preonset azimuthal structure is not uncommon in association with substorms [e.g., *Elphinstone et al.*, 1995; *Murphree and Johnson*, 1996]. The separation of two “beads” is approximately 0.4 h in local time, corresponding to an azimuthal mode number of 60. If mapped to $\sim 8 R_E$ into the equatorial magnetotail, the separation corresponds to ~ 5000 km. The latitude of 65° suggests that these structures mapped to the location of TH-C, using results from the analysis done in association with Figure 11. During the times when the UVI images were taken (Figure 13), TH-C initially recorded a westward (azimuthal) flow of <150 km/s, on which boundary (energetic plasma) modulations of 50–70 s were superposed (see the numbered lines above the first panel of TH-C in Figure 9 which correspond to the image times). To obtain a perturbation wavelength of 5000 km (which corresponds to the separation of the auroral beads), one would need to select a flow speed of 100 km/s and an oscillation period of 50 s, which are within the estimates obtained from TH-C. If these in situ perturbations created the smaller-scale auroral features, it is unclear why the perturbations recorded at TH-B, D, and A (see Figure 9 from 1110–1120 UT for TH-B) did not create such auroral features as well (also see section 7). It is also noted that the azimuthal structures appeared to be stationary during the period shown in the four images, vertical lines in Figure 13.

6. Ground Magnetic Pulsations

[26] A comparison of in situ measurements with ground magnetometer data also revealed one-to-one correlations. Figure 14 shows ion fluxes for different energy channels from TH-C and the H component from the high-latitude ground station KIAN (estimated to be closest to the foot point of TH-C), with both showing identical periodic oscillations over the entire time interval encompasses the preintensification and the intensification phases. In the preintensification phase (1110–1119 UT), period and amplitudes were significantly lower in space and on the ground than during the subsequent intensification phase. It is also noted that the correspondence during the preintensification phase exists for lower-energetic particles (top lines in first panel), whereas during the intensification phase it exists for the most energetic particles (bottom lines in first

Figure 12. (top) Comparison of ion injection data recorded by TH-C and auroral luminosity modulations (photon flux). The photon flux was averaged at 65° latitude, spanning the sector 2100 to 0000 MLT, which covers the region of auroral intensification. (bottom) Comparison of ion injection data recorded by TH-B and TH-D, and photon flux averaged at 68° and 69° latitude, spanning the sector 2100 to 0000 MLT.

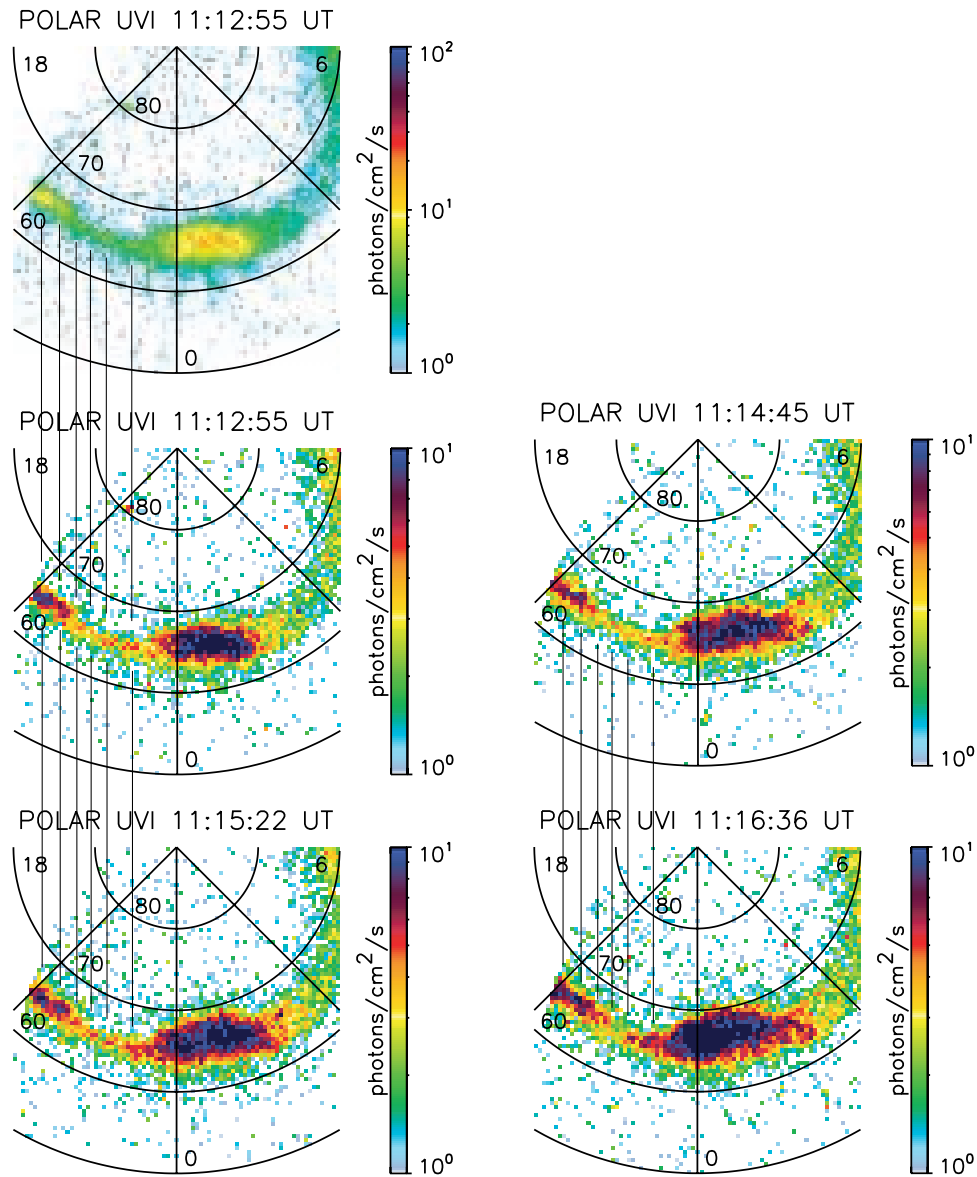


Figure 13. Polar-UVI images during the preintensification phase. Vertical lines are aligned with azimuthally spaced auroral forms. Note that the first and second images are identical but are shown with different color scales for comparison. See Figure 9 for a comparison with in situ measurements.

panel). Both pulsations fall within the Pi2 frequency band. Keiling *et al.* [2008] presented additional comparisons between midlatitude to low-latitude stations for the pulsations occurring during the intensification phase. The reader is cautioned that the upward pulse between 1118–1119 UT is an artifact from the detrending (see the unfiltered data in Figure 4e). The amplitude of the H component oscillation during the intensification phase was extremely large (~ 150 nT). Keiling *et al.* [2008] suggested that this large amplitude could mean that KIAN was observing a series of individual intensifications which yielded individual H -bay “pulses” at the Pi2 frequency.

[27] Figure 15 shows averaged photon fluxes of the two brightening regions, inside the auroral bulge at 65° and 68° – 69° , together with magnetometer data from KIAN and ZYK (located west of KIAN). The dashed lines reveal that the periodicity of the optical modulations is also manifested

in the magnetic field pulsations. Therefore, the ground magnetometer data suggest not only one SCW, but that additional current structures existed which modulated the optical aurora. These currents started at different times, pulsed out of phase, and mapped into different active regions in space, as inferred from the space-ground comparison of section 5.

7. Discussion

[28] Using data from six azimuthally and radially separated spacecraft, we have demonstrated the variability of plasma sheet activities, due to both temporal and spatial effects, during a substorm on 23 March 2007. First, the various plasma and magnetic field signatures showed significant differences for each spacecraft which can be attributed to their separations (i.e., each spacecraft probed a

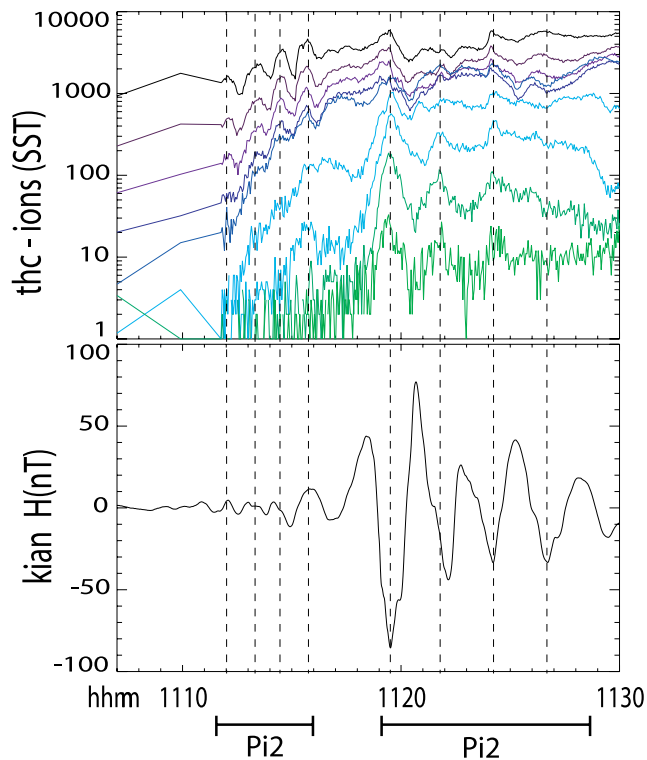


Figure 14. Comparison of ion flux enhancements at TH-C and ground pulsations before and after the intensification onset.

different plasma environment). Second, each spacecraft monitored the temporal substorm development from within different active plasma sheet regions. THEMIS was located beneath the neutral sheet and outside the current disruption region, which has high-frequency magnetic field fluctuations at onset [e.g., *Takahashi et al.*, 1987] and is typically thought to be of small azimuthal size ($\sim 1 R_E$) [*Ohtani et al.*, 1991]. Nevertheless, the spacecraft's locations (including LANL-97A) were favorable for determining several large-scale plasma sheet and plasma flow properties associated with the substorm. The substorm development was divided into a preintensification phase and an intensification phase. Low-frequency oscillations, both for particles and the magnetic field, were very prominent throughout both phases, and were approximately organized into a north-south and east-west motion. In addition, the most energetic particles showed an independent behavior. Having multiple spacecraft observations and a favorable constellation allowed us to create a 3-D picture of the near-Earth disturbances associated with the substorm.

[29] In addition, global auroral images provided simultaneous information on the auroral activity. The auroral oval showed typical preonset azimuthally structured forms along the oval [e.g., *Elphinstone et al.*, 1995], and the later developing auroral bulge showed well separated fine structure in the form of time-delayed auroral intensifications (illustrated in Figure 16). THEMIS was conjugate or near-conjugate to both preintensification and postintensification auroral features, thus allowing us to monitor the development of this auroral substorm/intensification from within the near-Earth plasma sheet.

[30] The following discussion of these and additional observations is organized into two subsections, which separately discuss the preintensification phase and the intensification phase.

7.1. Preintensification Phase

[31] During the preintensification phase (which temporally coincided with a smaller substorm expansion phase occurring farther east), the THEMIS spacecraft periodically skimmed the boundary of energized, and increasingly energized, plasma regions that were horizontally layered (X-Y GSM plane) and superposed with wave-like perturbations moving westward, as illustrated in Figure 17. These combined motions could be considered surface waves at the boundary separating the hot plasma region from colder surroundings. The surface wave showed a gradual energization of the hot plasma region that could be driven by the Kelvin-Helmholtz instability (KHI). KHI requires a velocity layer [e.g., *Voronkov et al.*, 1997], and it was suggestive that such a shear layer existed inside the boundary that was skimmed by the spacecraft.

[32] From radially separated THEMIS spacecraft, we found that different oscillation/wave periods were present at different radial distances (Figure 17). The increase in

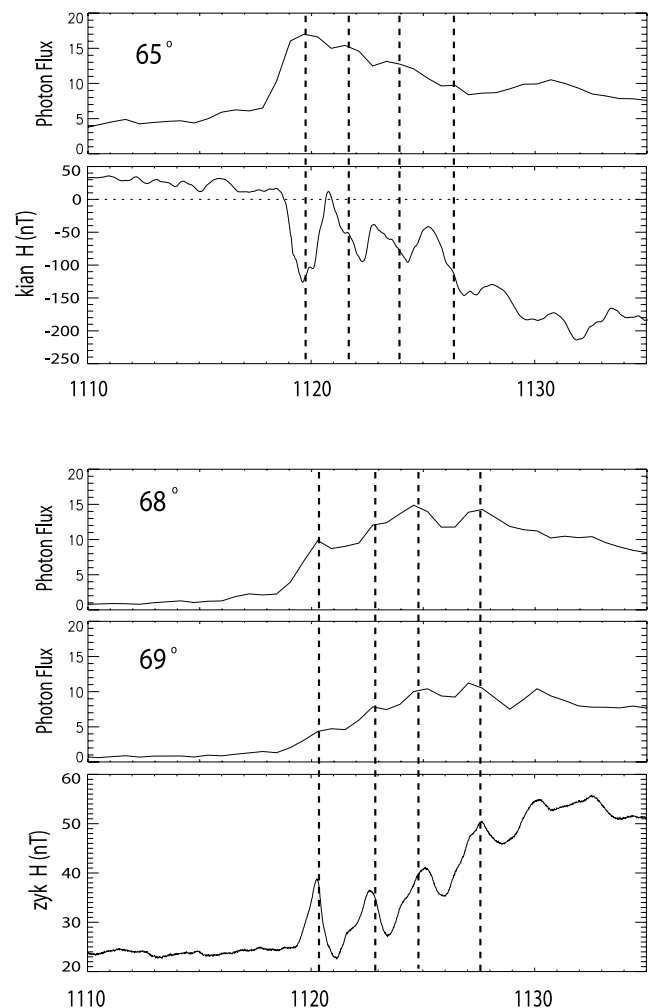


Figure 15. Comparison of averaged photon fluxes (same as in Figure 11) with unfiltered ground magnetometer data.

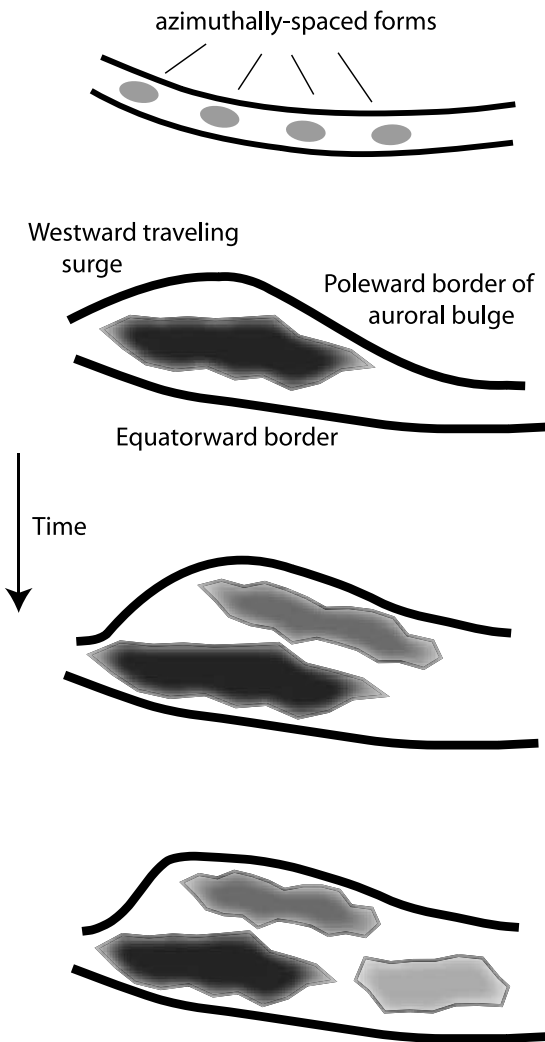


Figure 16. Cartoon of the temporal evolution of the auroral bulge associated with the preintensification and intensification phases on 23 March 2007.

period with increasing radial distance could be due to the different cross-sectional area of the current sheet layer at each distance. They could also indicate the presence of separate regions in the current sheet (e.g., filamentary structures [Schindler and Ness, 1972]). The existence of distinct regions is further supported by the different onset times of activity at each region. Two spacecraft (LANL-97A, TH-E) did not record any preoscillations, possibly because they were located outside of the active regions, which is further confirmed by the dispersed ion injection signatures at both locations, associated with the main ion injections that followed the preintensification phase (see section 7.2). In contrast, the other spacecraft (TH-A, B, C, and D) which recorded oscillations during the preintensification phase recorded dispersionless ion injections in the intensification phase. This further suggests that the preintensification oscillations were associated with, and possibly causally related to, the onset of the main ion injections.

[33] The low-frequency magnetic field and particle oscillations reported here resemble those reported by Roux *et al.* [1991] and Holter *et al.* [1995], who investigated the same

substorm using GEOS 2 data. During early breakup, field oscillations with periods of 45–65 s were followed by oscillations with a period of 300 s. This is in particular similar to TH-C which initially recorded ~1-min oscillations followed by 135-s oscillations. Roux *et al.* [1991], using single spacecraft measurements, interpreted these oscillations as westward propagating waves. The propagation speed was estimated to be ~100 km/s, using the assumption that the waves propagated at the ion drift speed. Using multiple spacecraft, our study provided evidence that such oscillations/waves can vary with radial separation. The significance of preonset oscillations was also reported by, for example, Ohtani *et al.* [1992], who identified a magnetic field perturbation immediately preceding (by ~30 s) substorm onset that grew “explosive”-like, and the authors argued that it may be critical in triggering substorm onset. Cheng and Lui [1998] expanded their analysis by arguing that a low-frequency instability in the Pi2 range was excited ~2 min before onset, which led into this explosive growth. Erickson *et al.* [2000] reported quasi-electrostatic oscillations during the growth phase and before onset, calling them trigger waves, and also suggested that these oscillations play a role in triggering the main onset.

[34] The preintensification phase itself was preceded by a pseudobreakup, which left its mark in the form of pulsation activity at the spacecraft locations. The transition from pseudobreakup to preintensification was observed as an intensification in wave amplitude (up to dB/B = 35%), followed by a gradual decrease in frequency. A decreasing frequency was also observed during the transition from preintensification to intensification phase. A shift toward shorter frequency, associated with substorm activation in the near-Earth plasma sheet, was also reported by Lui and Najmi [1997].

[35] Other observations that may be significant for determining the onset mechanism were the apparent, but not certain, harmonically related double frequencies (76 and 167 s) recorded at TH-C. Holter *et al.* [1995] argued for such a relationship for observed 300-s and 600-s oscillations

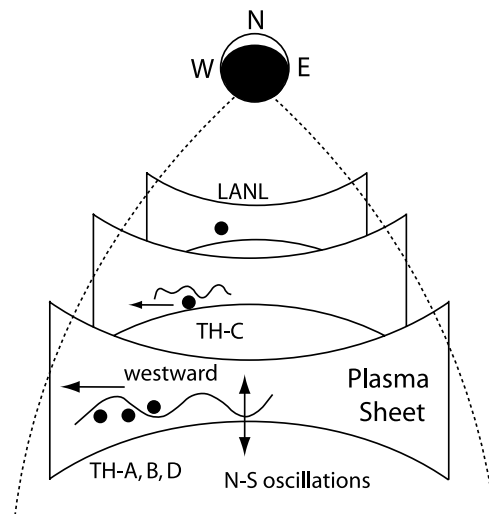


Figure 17. Schematic illustration of north-south oscillations in different planes along the magnetotail, superposed on an azimuthal drift. Spacecraft locations are labeled.

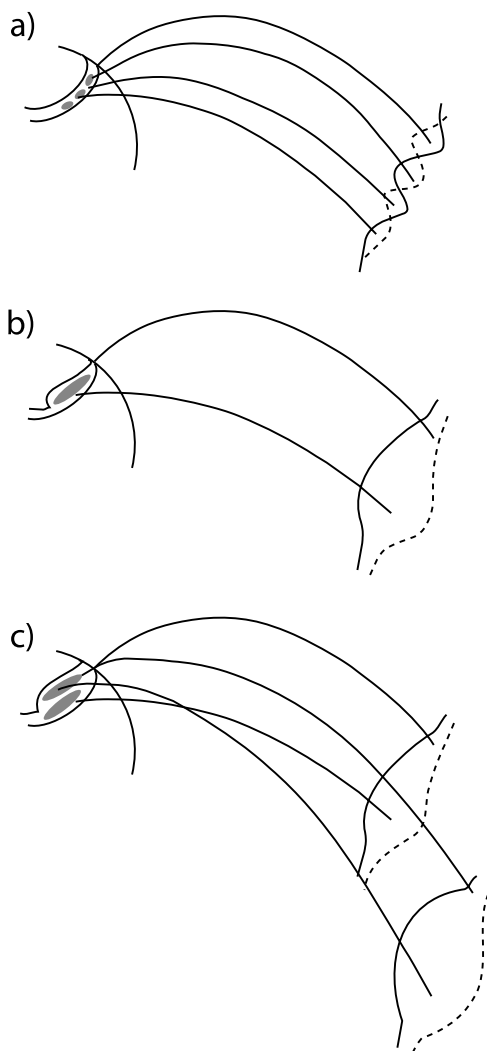


Figure 18. Temporal evolution of the auroral fine structure inside the auroral bulge on 23 March 2007 and their connections to different regions in space.

during a substorm. *Voronkov* [2005] reported simulated harmonics, in association with substorms, in a cavity in the near-Earth plasma sheet that led to nonlinear ballooning eigenmodes. However, the estimated oscillation periods were lower than those observed here.

[36] Simultaneous with the preintensification oscillations at THEMIS, the aurora showed azimuthally spaced forms (“beads”) at the location of the subsequent brightening of the auroral intensification (as illustrated in Figure 16). Shortly before intensification, these auroral forms turned into an elongated auroral structure, which then grew into the first intensification region of the auroral bulge. That TH-C was conjugate to these auroral forms, or more precisely, that it was periodically immersed into the conjugate region is possible, not only because of the footpoint mapping (see Figure 3) but also because of the following observations: (1) during the azimuthally spaced auroral forms, TH-C recorded drifting perturbations (surface waves) at an energized plasma boundary; (2) these perturbations disappeared with the azimuthally spaced auroral forms; (3) the

spatial dimensions of the auroral forms were comparable to the in situ wavelength when mapped along magnetic field lines; and (4) ground Pi2 were one-to-one correlated with the boundary perturbations observed at TH-C. To explain the azimuthally spaced auroral forms before the intensification phase, we adopt the scenario proposed by *Roux et al.* [1991], who applied it to the breakup phase, but it can also be applied during the preintensification phase. The idea of this scenario is that the boundary perturbations (surface waves) are coupled via field-aligned currents to the azimuthally spaced auroral forms. *Roux et al.* [1991, Figure 10] illustrated how such a structure could lead to a charge separation, that could then flow along field lines into the ionosphere. Hence, each wavelength essentially forms a small current wedge that can, under the right ionospheric conditions, lead to auroral brightening. Therefore, it is conceivable that these small current wedges created the auroral fine structure, as illustrated in Figure 18a. Although the other spacecraft (TH-D, A, and B) also recorded wave-like structures, there appeared to be no azimuthally spaced auroral forms conjugate to them. One reason may be different ionospheric conditions, but this has not been confirmed. It is also not clear why the azimuthally spaced auroral forms remained stationary for the duration of the preintensification oscillations while the boundary perturbations were drifting.

7.2. Intensification Phase

[37] The intensification phase was initiated on the ground by the brightening of a faint preexisting elongated auroral form which showed an azimuthally spaced fine structure shortly before breakup. In space, THEMIS and LANL-97A recorded dispersionless and dispersive injections of energetic (>100 keV) ions. Dispersionless injections were only recorded by those spacecraft (TH-C, D, A, and B) that also recorded preintensification oscillations, suggesting that these oscillations played a role in the initiation of the intensification. TH-E, on the other hand, did not record any preintensification oscillations, and only recorded energy-dispersed injections at a later time, possibly due to their drift from the injection site near TH-B, D, and A. In a similar fashion, LANL-97A, located closer to Earth, did not record preintensification oscillations, and only recorded energy-dispersed, time-delayed injections with respect to TH-C, giving further support that preintensification oscillations played a role in the onset. Such a role has been associated with the ballooning mode scenario of substorm breakup [e.g., *Roux et al.*, 1991; *Cheng and Lui*, 1998].

[38] In this study, the main ion injections recorded by the six spacecraft were grouped into two groups, according to their periodic behavior. The most striking result of this study was that differences in the ion energy flux between the two groups of spacecraft were correlated with data on the ground, namely auroral modulations and ground pulsations. In addition to the first auroral intensification region, the expanding auroral bulge developed two more spatially separated regions of intense aurora, which followed within minutes (illustrated in Figure 16). The auroral regions were modulated in intensity with periods of approximately 100–150 s and were oscillating out of phase. Ground pulsations were one-to-one correlated with the auroral modulations. The auroral regions were magnetically

connected to the two spacecraft groups, which we inferred from the onset time and the identical periodic behavior, in addition to model mapping. Thus, the ground data possibly suggest not only one wedge-like current system but the existence of additional current structures (as illustrated in Figure 18c). These currents started at different times in different locations of the near-Earth plasma sheet and pulsed out of phase. Connected to the ionosphere through magnetic field lines, they then drove the simultaneous ground and ionospheric activities reported here. Roux *et al.* [1991] reported such a connection for one space region and the westward traveling surge in the ionosphere. By analogy, it can be suggested that a third region must have existed in space which was conjugate to the third auroral intensification region (as illustrated in Figure 1). However, no spacecraft was inside this speculated region of space to monitor its behavior. We also point out that differences in the dipolarization signature for both groups were likely the result of Group 1 being further below the neutral sheet than Group 2, resulting in a weaker dipolarization signature.

[39] A very clear signature of this substorm was that the westward expansion of the substorm did not occur continuously but in discrete steps in the form of new brightening regions at different locations. Such step-like behavior inside the auroral bulge has been reported by others [e.g., Sergeev and Yahnin, 1979], and it was proposed that each intensification may be connected to different regions in the plasma sheet, although observational evidence has not been given so far. The progression of active regions in the auroral bulge could be due to multiple disruption sites developing at progressively further downstream distances [e.g., Lui, 1996, and references therein], albeit for our event the third activation occurred closer to Earth than the second one. Alternatively, one might be tempted to argue that external periodic plasma flows [e.g., Kepko and Kivelson, 1999] could be responsible for the periodic ion injections and the correlated optical modulations reported here; however, no spacecraft data were available to monitor the plasma flow in the current sheet further down tail. On the other hand, we reported not only one, but two, different regions in space that oscillated out of phase. This out-of-phase behavior cannot, in our view, be driven by alternating BBFs which happen to have the same temporal periodicity. Instead, we find it more likely that a wave phenomenon, such as a ballooning mode, operated at two locations. The pronounced oscillatory signatures of the magnetic field and particles throughout our event also support this conjecture. Because the two space regions were oscillating nearly out of phase with the same average period, it seems likely that the space regions were still physically connected. As also noted, while the intensity of one conjugate auroral region steadily decreased, the intensity of the other one steadily increased as if the energy shifted in a coupled system from one region to the other. Nevertheless, we could not conclusively verify whether the two space regions were indeed physically coupled, or whether they were simply oscillating independently.

[40] At intensification onset, Group 2 of the THEMIS spacecraft recorded an abrupt increase of flow velocity (up to 350 km/s) for less than 30 s followed by a rotation of the flow vector (i.e., vortex). This rotation was followed by periodic and fairly regular oscillations in the X-Y plane (i.e.,

sloshing) that lasted for more than 10 min after which the oscillations started to become more irregular. Although similar, Group 1 recorded this abrupt increase 1–2 min before the main injections, which nearly coincided with the formation of the preintensification “arc.” It is tempting to associate these sudden flow increases and the following sloshing motion with the sudden ballooning, which can create vortical structures [e.g., Voronkov, 2005]. The vortex recorded by Group 2 was clockwise (i.e., positive vortex) and therefore associated with upward currents [Borovsky and Bonnell, 2001]. It can thus be suggested that these upward currents were associated with the brightening in the auroral bulge. We also note that TH-C recorded upward flowing ions (reported by Keiling *et al.* [2008]) which is consistent with an upward current region and auroral activity.

[41] Finally, it was noted that the most energetic particles (>100 keV) did not follow the motion of the bulk plasma (see Keiling *et al.* [2008] for additional evidence). The ground pulsations and optical modulations during the intensification phase were correlated with those energetic ions, in contrast to the preintensification oscillations where the lower-energetic particles (<100 keV) were correlated with ground pulsations. Therefore, owing to the different energies of the correlated particles before and after intensification onset, it is likely that they coupled to the ground in different ways. For example, Keiling *et al.* [2008] suggested that the periodic energetic (>100 keV) ion injections at TH-C caused individual substorm bays on the ground, yielding the extremely large ($\delta H = \sim 150$ nT) ground amplitudes, that happened to be in the Pi2 range. In contrast, the small-amplitude Pi2 before intensification were correlated with the oscillations of the bulk plasma sheet. It has previously been suggested that neutral sheet oscillations cause ground Pi2s [Bauer *et al.*, 1995a; Maynard *et al.*, 1996; Erickson *et al.*, 2000] but no one-to-one correlations were shown.

8. Conclusions

[42] The 23 March 2007 substorm showed a very intricate, but not unusual, auroral signature with azimuthally spaced auroral forms and multiple time-delayed intensifications inside the poleward expanding auroral bulge. The novel result presented here was the correlation of two auroral intensification regions and conjugate in situ measurements, simultaneously recorded in two space regions as illustrated in Figure 18. The first brightening region showed an azimuthal extension and grew out of a preexisting elongated auroral form, possibly an auroral arc. Within tens of seconds, a second auroral brightening region formed poleward. Both regions were optically modulated out of phase. We provided evidence that both regions were connected to two separated regions in the near-Earth plasma sheet which periodically energized ions. The same periodicity was also observed in simultaneous ground pulsations. Important, in our opinion, is that the proposed conjugacy between the optical aurora and the two space regions was not only based on field line mapping, still a challenging and controversial task, but also confirmed via these one-to-one correlated periodic signatures.

[43] The two out-of-phase oscillating space regions represent a topological constraint which suggests that a local

wave phenomenon (such as a ballooning-type mode) caused the onset of the intensifications and their subsequent developments, rather than directly driven BBF activations. Preonset, wave-like plasma sheet structures (moving westward and possibly causing the azimuthally structured auroral forms) support the suggestion of a wave phenomenon. Owing to the locations of the THEMIS spacecraft below the onset region in the plasma sheet, it was not possible to assess some of the physical parameters needed to evaluate the type of wave phenomenon. Nevertheless, a qualitative explanation for some of the reported features can be attempted within the framework of the ballooning mode. This mode is thought to exist in the region that separates dipolar-like from tail-like field lines [e.g., Cheng, 2004, and references therein]. Under the right physical conditions, a disturbance can grow into a wave-like structure that moves westward [e.g., Roux *et al.*, 1991]. This growth can be driven by plasma shear flow [e.g., Voronkov *et al.*, 1997] but other scenarios are also possible. This growth has been argued to amplify explosively [Ohtani *et al.*, 1992], followed by a cross-tail current disruption and the development of a substorm. Furthermore, at substorm onset and intensification, it is generally thought that the plasma sheet expands (i.e., increases its volume), or, equivalently, the current sheet thickens. Observations reported here for the 23 March 2007 substorm that agree with the scenario, and some additional noteworthy observations, were the following:

[44] 1. The plasma oscillation and the magnetic field showed a diamagnetic relationship. Such a relationship leads to local plasma pressure changes, which have been associated with a ballooning-type mode [e.g., Miura *et al.*, 1989; Ohtani and Tamao, 1993; Bhattacharjee *et al.*, 1998].

[45] 2. Simultaneous with the onset of pseudobreakup oscillations, the total magnetic field started to increase. No spacecraft observations were available further down the tail to verify or exclude the existence of fast plasma flows which might have carried magnetic flux toward Earth. If the flows existed, the associated magnetic flux transport may have preconditioned the region for the subsequent wave-type phenomenon.

[46] 3. The preintensification oscillations showed a gradual energization of the plasma which could be driven by the Kelvin-Helmholtz instability, and which in turn, could trigger a ballooning instability. Some evidence for a velocity shear layer existed. Such a hybrid mode has, for example, been numerically modeled by Voronkov *et al.* [1997].

[47] 4. The azimuthal flow turned into a vortex at the time of dipolarization in one group of spacecraft which has also been associated, although not exclusively, with the ballooning mode [e.g., Voronkov, 2005].

[48] 5. The vortex was clockwise (i.e., positive vortex) and was thus associated with upward currents. Therefore, it can be suggested that these upward currents were associated with the brightening in the auroral bulge.

[49] 6. The change to a longer oscillation period at intensification onset, observed by THEMIS, could be related to a thickening of the plasma sheet since an expanded plasma sheet would provide a larger region for oscillations, which increases the inherent oscillation period of this region. Also noted was that the spacecraft penetrated deeper

into the hot plasma region during the intensification, as opposed to before intensification, supporting the scenario of a thicker current sheet.

[50] 7. Preintensification oscillations were correlated with ground Pi2, which could be achieved by a coupling of the drifting waves to a field-guided wave mode.

[51] 8. The modulations of the intensification injections could be related to the oscillations of a large-scale wave that periodically energized the particles. These particle modulations were also in the Pi2 range, which has been associated with a ballooning mode [e.g., Cheng, 2004].

[52] 9. Puzzling was the finding of a possible coupling for the two space regions that executed out-of-phase oscillations. Whether such behavior can be explained within the framework of the ballooning mode remains to be seen.

[53] **Acknowledgments.** This work was supported by the NASA THEMIS project. The work of the IGEP team at the Technical University of Braunschweig was financially supported by the German Ministerium für Wirtschaft und Technologie and the German Zentrum für Luft- und Raumfahrt under grant 50QP0402. We thank the LANL and the 210 MM (K. Yumoto and K. Shiokawa) science teams for making their data available.

[54] Amitava Bhattacharjee thanks Igor Voronkov and another reviewer for their assistance in evaluating this paper.

References

- Angelopoulos, V. (2008), The THEMIS mission, *Space Sci. Rev.*, doi:10.1007/s11214-008-9336-1, in press.
- Angelopoulos, V., C. F. Kennel, F. V. Coroniti, R. Pellat, M. G. Kivelson, R. J. Walker, C. T. Russell, W. Baumjohann, W. C. Feldman, and J. T. Gosling (1994), Statistical characteristics of bursty bulk flow events, *J. Geophys. Res.*, *99*, 21,257–21,280, doi:10.1029/94JA01263.
- Angelopoulos, V., *et al.* (2008), First results from the THEMIS mission, *Space Sci. Rev.*, doi:10.1007/s11214-008-9378-4, in press.
- Auster, H. U., *et al.* (2008), The THEMIS fluxgate magnetometer, *Space Sci. Rev.*, doi:10.1007/s11214-008-9365-9, in press.
- Bauer, T. M., W. Baumjohann, and R. A. Treumann (1995a), Neutral sheet oscillations at substorm onset, *J. Geophys. Res.*, *100*, 23,737–23,742, doi:10.1029/95JA02448.
- Bauer, T. M., W. Baumjohann, R. A. Treumann, N. Sckopke, and H. Lühr (1995b), Low-frequency waves in the near-Earth plasma sheet, *J. Geophys. Res.*, *100*, 9605–9617, doi:10.1029/95JA00136.
- Baumjohann, W., and K.-H. Glassmeier (1984), The transient response mechanism and Pi2 pulsations at substorm onset: Review and outlook, *Planet. Space Sci.*, *32*, 1361–1370, doi:10.1016/0032-0633(84)90079-5.
- Bester, M., M. Lewis, B. Roberts, J. McDonald, D. Pease, J. Thorsness, S. Frey, D. Cosgrove, and D. Rummel (2008), THEMIS operations, *Space Sci. Rev.*, doi:10.1007/s11214-008-9456-7, in press.
- Bhattacharjee, A., Z. W. Ma, and X. Wang (1998), Ballooning instability of a thin current sheet in the high-Lundquist-number magnetotail, *Geophys. Res. Lett.*, *25*, 861–864, doi:10.1029/98GL00412.
- Borovsky, J. E., and J. Bonnell (2001), The DC electrical coupling of flow vortices and flow channels in the magnetosphere to the resistive ionosphere, *J. Geophys. Res.*, *106*, 28,967–28,994, doi:10.1029/1999JA000245.
- Cheng, C. Z. (1991), A kinetic-magnetohydrodynamic model for low-frequency phenomena, *J. Geophys. Res.*, *96*, 21,159–21,171, doi:10.1029/91JA01981.
- Cheng, C. Z. (2004), Physics of substorm growth phase, onset, and dipolarization, *Space Sci. Rev.*, *113*, 207–270, doi:10.1023/B:SPAC.0000042943.59976.0e.
- Cheng, C. Z., and A. T. Y. Lui (1998), Kinetic ballooning instability for substorm onset and current disruption observed by AMPTE/CCE, *Geophys. Res. Lett.*, *25*, 4091–4094, doi:10.1029/1998GL900093.
- Elphinstone, R. D., *et al.* (1995), Observations in the vicinity of substorm onset: Implications for the substorm process, *J. Geophys. Res.*, *100*, 7937–7969, doi:10.1029/94JA02938.
- Erickson, G. M., N. C. Maynard, W. J. Burke, G. R. Wilson, and M. A. Heinemann (2000), Electromagnetics of substorm onsets in the near-geosynchronous plasma sheet, *J. Geophys. Res.*, *105*, 25,265–25,290, doi:10.1029/1999JA000424.
- Friedrich, E., *et al.* (2001), Ground-based observations and plasma instabilities in auroral substorms, *Phys. Plasmas*, *8*, 1104–1110, doi:10.1063/1.1355678.

- Holter, Ø., C. Altman, A. Roux, S. Perraut, A. Pedersen, H. Pécseli, B. Lybekk, J. Trulsen, A. Korth, and G. Kremser (1995), Characterization of low frequency oscillations at substorm breakup, *J. Geophys. Res.*, *100*, 19,109–19,119, doi:10.1029/95JA00990.
- Hughes, W. J., and R. J. L. Grard (1984), A second harmonic geomagnetic field line resonance at the inner edge of the plasma sheet: GEOS 1, ISEE 1, and ISEE 2 observations, *J. Geophys. Res.*, *89*, 2755–2764, doi:10.1029/JA089iA05p02755.
- Keiling, A., J. R. Wygant, C. Cattell, K.-H. Kim, C. T. Russell, D. K. Milling, M. Temerin, F. S. Mozer, and C. A. Kletzing (2001), Pi2 pulsations observed with the Polar satellite and ground stations: Coupling of trapped and propagating fast mode waves to a midlatitude field line resonance, *J. Geophys. Res.*, *106*, 25,891–25,904, doi:10.1029/2001JA900082.
- Keiling, A., et al. (2008), Correlation of substorm injections, auroral modulations, and ground Pi2, *Geophys. Res. Lett.*, *35*, L17S22, doi:10.1029/2008GL033969.
- Kennel, C. F. (1995), *Convection and Substorms: Paradigms of Magnetospheric Phenomenology*, *Int. Ser. on Astron. Astrophys.*, vol. 2, Oxford Univ. Press, New York.
- Kepko, L., and M. G. Kivelson (1999), Generation of Pi2 pulsations by bursty bulk flows, *J. Geophys. Res.*, *104*, 25,021–25,034, doi:10.1029/1999JA900361.
- Lessard, M. R., M. K. Hudson, J. C. Samson, and J. R. Wygant (1999), Simultaneous satellite and ground-based observations of a discretely driven field line resonance, *J. Geophys. Res.*, *104*, 12,361–12,377, doi:10.1029/1998JA900117.
- Liu, W., X. Li, T. E. Sarris, C. Cully, R. E. Ergun, V. Angelopoulos, D. E. Larson, A. Keiling, K. H. Glassmeier, and H. U. Auster (2008), Observation and modeling of the injection observed by THEMIS and LANL satellites during 23 March 2007 substorm event, *J. Geophys. Res.*, doi:10.1029/2008JA013498, in press.
- Lui, A. T. Y. (1996), Current disruption in the Earth's magnetosphere: Observations and models, *J. Geophys. Res.*, *101*, 13,067–13,088, doi:10.1029/96JA00079.
- Lui, A. T. Y., and A.-H. Najmi (1997), Time-frequency decomposition of signals in a current disruption event, *Geophys. Res. Lett.*, *24*, 3157–3160, doi:10.1029/97GL03229.
- Lui, A. T. Y., R. E. Lopez, B. J. Anderson, K. Takahashi, L. J. Zanetti, R. W. McEntire, T. A. Potemra, D. M. Klumpner, E. M. Greene, and R. Strangeway (1992), Current disruptions in the near-Earth neutral sheet region, *J. Geophys. Res.*, *97*, 1461–1480, doi:10.1029/91JA02401.
- Lui, A. T. Y., K. Liou, M. Nosé, S. Ohtani, D. J. Williams, T. Mukai, K. Tsuruda, and S. Kokubun (1999), Near-Earth dipolarization: Evidence for a non-MHD process, *Geophys. Res. Lett.*, *26*, 2905–2908, doi:10.1029/1999GL003620.
- Maynard, N. C., W. J. Burke, E. M. Basinska, G. M. Erickson, W. J. Hughes, H. J. Singer, A. G. Yahnin, D. A. Hardy, and F. S. Mozer (1996), Dynamics of the inner magnetosphere near times of substorm onsets, *J. Geophys. Res.*, *101*, 7705–7736, doi:10.1029/95JA03856.
- McFadden, J. P., C. W. Carlson, D. Larson, V. Angelopoulos, M. Ludlam, R. Abiad, and B. Elliot (2008), The THEMIS ESA plasma instrument and in-flight calibration, *Space Sci. Rev.*, doi:10.1107/s11214-008-9440-2, in press.
- Miura, A., S. Ohtani, and T. Tamao (1989), Ballooning instability and structure of diamagnetic hydromagnetic waves in a model magnetosphere, *J. Geophys. Res.*, *94*, 15,231–15,242, doi:10.1029/JA094iA11p15231.
- Murphree, J. S., and M. L. Johnson (1996), Clues to plasma processes based on Freja UV observations, *Adv. Space Res.*, *18*, 95–105, doi:10.1016/0273-1177(95)00973-6.
- Ohtani, S., and T. Tamao (1993), Does the ballooning instability trigger substorms in the near-Earth magnetotail?, *J. Geophys. Res.*, *98*, 19,369–19,379, doi:10.1029/93JA01746.
- Ohtani, S., K. Takahashi, L. J. Zanetti, T. A. Potemra, R. W. McEntire, and T. Iijima (1991), Tail current disruption in the geosynchronous region, in *Magnetospheric Substorms*, *Geophys. Monogr. Ser.*, vol. 64, edited by J. R. Kan et al., pp. 131–137, AGU, Washington, D. C.
- Ohtani, S., K. Takahashi, L. J. Zanetti, T. A. Potemra, R. W. McEntire, and T. Iijima (1992), Initial signatures of magnetic field and energetic particle fluxes at tail reconfiguration: Explosive growth phase, *J. Geophys. Res.*, *97*, 19,311–19,324, doi:10.1029/92JA01832.
- Raeder, J., D. Larson, W. Li, L. Kepko, and T. Fuller-Rowell (2008), Open GGCM simulations for the THEMIS mission, *Space Sci. Rev.*, doi:10.1007/s11214-008-9421-5, in press.
- Rankin, R., J. C. Samson, and V. T. Tikhonchuk (1999), Discrete auroral arcs and nonlinear dispersive field line resonances, *Geophys. Res. Lett.*, *26*, 663–666, doi:10.1029/1999GL900058.
- Roux, A., S. Perraut, P. Robert, A. Morane, A. Pedersen, A. Korth, G. Kremser, B. Aparicio, D. Rodgers, and R. Pellinen (1991), Plasma sheet instability related to the westward traveling surge, *J. Geophys. Res.*, *96*, 17,697–17,714, doi:10.1029/91JA01106.
- Runov, A., R. Nakamura, W. Baumjohann, T. L. Zhang, M. Volwerk, H.-U. Eichelberger, and A. Balogh (2003), Cluster observation of a bifurcated current sheet, *Geophys. Res. Lett.*, *30*(2), 1036, doi:10.1029/2002GL016136.
- Ruohoniemi, J. M., R. A. Greenwald, K. B. Baker, and J. C. Samson (1991), HF radar observations of Pc5 field line resonances in the mid-night/early morning MLT sector, *J. Geophys. Res.*, *96*, 15,697–15,710, doi:10.1029/91JA00795.
- Russell, C. T., P. J. Chi, D. J. Dearborn, Y. S. Ge, B. Kuo-Tiong, J. D. Means, D. R. Pierce, K. M. Rowe, and R. C. Snare (2008), THEMIS ground-based magnetometers, *Space Sci. Rev.*, doi:10.1007/s11214-008-9337-0, in press.
- Samson, J. C., T. J. Hughes, F. Creutzberg, D. D. Wallis, R. A. Greenwald, and J. M. Ruohoniemi (1991), Observations of a detached discrete arc in association with field line resonances, *J. Geophys. Res.*, *96*, 15,683–15,695, doi:10.1029/91JA00796.
- Samson, J. C., D. D. Wallis, T. J. Hughes, F. Creutzberg, J. M. Ruohoniemi, and R. A. Greenwald (1992), Substorm intensification and field line resonances in the nightside magnetosphere, *J. Geophys. Res.*, *97*, 8495–8518, doi:10.1029/91JA03156.
- Samson, J. C., R. Rankin, and V. Tikhonchuk (2003), Optical signatures of auroral arcs produced by field-line resonances: Comparison with satellite observations and modeling, *Ann. Geophys.*, *21*, 933–945.
- Schindler, K., and N. F. Ness (1972), Internal structure of the geomagnetic neutral sheet, *J. Geophys. Res.*, *77*, 91–100, doi:10.1029/JA077i001p00091.
- Sergeev, V. (1974), On the longitudinal localization of the substorm active region and its changes during the substorm, *Planet. Space Sci.*, *22*, 1341, doi:10.1016/0032-0633(74)90055-5.
- Sergeev, V. A., and A. G. Yahnin (1979), The features of auroral bulge expansion, *Planet. Space Sci.*, *27*, 1429–1440, doi:10.1016/0032-0633(79)90089-8.
- Sergeev, V., et al. (2003), Current sheet flapping motion and structure observed by Cluster, *Geophys. Res. Lett.*, *30*(6), 1327, doi:10.1029/2002GL016500.
- Sibeck, D. G., and V. Angelopoulos (2008), THEMIS science objectives and mission phases, *Space Sci. Rev.*, doi:10.1007/s11214-008-9393-5, in press.
- Sonnerup, B. U. O., and L. J. Cahill (1968), Explorer 12 observations of the magnetopause current layer, *J. Geophys. Res.*, *73*, 1757–1770, doi:10.1029/JA073i005p01757.
- Takahashi, K., L. J. Zanetti, R. E. Lopez, R. W. McEntire, T. A. Potemra, and K. Yumoto (1987), Disruption of the magnetotail current sheet observed by AMPTE/CCE, *Geophys. Res. Lett.*, *14*, 1019–1022, doi:10.1029/GL014i010p01019.
- Torr, M. R., et al. (1995), A far ultraviolet imager for the International Solar Terrestrial Physics Mission, in *The Global Geospace Mission*, edited by C. T. Russell, pp. 459–495, Kluwer Acad., Norwell, Mass.
- Voronkov, I. O. (2005), Near-Earth breakup triggered by the earthward traveling burst flow, *Geophys. Res. Lett.*, *32*, L13107, doi:10.1029/2005GL022983.
- Voronkov, I., R. Rankin, P. Frycz, V. T. Tikhonchuk, and J. C. Samson (1997), Coupling of shear flow and pressure gradient instabilities, *J. Geophys. Res.*, *102*, 9639–9650, doi:10.1029/97JA00386.
- Wanliss, J. A., and R. Rankin (2002), Auroral substorm dynamics and field line resonances, *Earth Planets Space*, *54*, 927–932.
- Yumoto, K., and the 210° MM Magnetic Observation Group (1996), The STEP 210° magnetic meridian network project, *J. Geomagn. Geoelectr.*, *48*, 1297–1309.
- Ziesolleck, C. W. S., and D. R. McDiarmid (1994), Auroral latitude Pc5 field line resonance: Quantized frequencies, spatial characteristics, and diurnal variation, *J. Geophys. Res.*, *99*, 5817–5830, doi:10.1029/93JA02903.

V. Angelopoulos, C. Carlson, M. Fillingim, S. Frey, A. Keiling, D. Larson, J. McFadden, and G. Parks, Space Sciences Laboratory, University of California, Berkeley, CA 94720-7450, USA. (keiling@ssl.berkeley.edu)

H. U. Auster and K.-H. Glassmeier, Technische Universität Braunschweig, D-38106 Braunschweig, Germany.

X. Li and W. Liu, Laboratory for Atmospheric and Space Physics, University of Colorado, Boulder, CO 80303, USA.

W. Magnes, Space Research Institute, Austrian Academy of Science, 8042 Graz, Austria.